Addis Ababa University

Addis Ababa Institute of Technology

School Of Mechanical and Industrial Engineering

Graduate Program in Rolling Stock Engineering

SIMULATION OF CRACK PROPAGATION OF A SKIDDED RAIL WHEEL USING EXTENDED FINITE ELEMENT METHOD (XFEM)

A Thesis submitted to the school of Mechanical and Industrial graduate studies in Partial fulfillment of the Degree of Master of science in Mechanical (Rolling-Stock) Engineering

By: Natnael Mandefro

Advisor

Dr. Daniel Tilahun

March, 2016

ADDIS ABABA, ETHIOPIA

Simulation of crack propagation of a skidded rail wheel using Extended Finite Element Method (XFEM)
Master's Thesis in Mechanical (Rolling stock) Engineering
NATNAEL MANDEFRO
Department of Mechanical and Industrial Engineering
Addis Ababa Institute of Technology

Abstract

In this thesis work, an investigation of a crack growth pattern due to the additional effect of the frictional heat induced on the static mechanical full load due to skidding of a wheel on a rail is conducted using an Extended Finite Element Method (XFEM).

The contact parameters are determined using Hertz contact theory. The assumption of the elliptical contact pressure distribution is linearized to give a simple rectangular pressure distribution. The contact elliptical area is also assumed to be as an equivalent rectangular area. The frictional heating case is considered at the maximum sliding velocity having in mind the full loading spectrum of the wheel on the entire journey. The Material of the wheel is assumed to be an isotropic hardened Elastic-plastic material and the damage initiation criterion selected is the maximum principal stress. An energy based damage evolution is selected for the crack growth simulation.

The crack Extension pattern with respect to the crack tip maximum principal stress and Equivalent plastic strain (PEEQ) are plotted for both case scenarios and it is can then be inferred that the as the crack length increases the crack tip stress and plastic strain also increases therefore the wheel will lose integrity for further successive damage.

Keywords: *Crack propagation, Elastic-Plastic, Frictional Heating, Hertz contact Theory, Extended finite Element Method (XFEM), Maximum principal stress, Equivalent plastic strain (PEEQ).*

Acknowledgements

All praise and thanks to the Almighty God for everything he gave me in every step of my life which cannot be mentioned in words by the name of his son Christ Jesus.

I want to convey my special thanks to my thesis advisor Dr. Daniel Tilahun Redda in giving me some valuable points from the title and finalization of this thesis paper along with his plenty of responsibilities for the department. It gives me immense pleasure to thank Ato Behailu Zewde (PhD candidate) in showing the importance of such research topic and supply me materials for laying foundation of fracture mechanics science in me. And my sincere gratitude goes to Ato Mulugeta Hailemariam (PhD candidate) who guided me along the track of crack analysis, good thesis output result and supports me in using ABAQUS software.

I am also grateful to thank all my friends and those who always gave me fruitful suggestions and shared their knowledge with me.

Table of Contents

Page

List of Figures

List of Tables

Nomenclatures

a	Lateral semi-axis length of the elliptical contact	[mm]
b	Longitudinal semi-axis length of the elliptical contact	[mm]
D	Wheel diameter	[mm]
δ	Heat Penetration depth	[µm]
L	Péclet Number	[-]
V_s	Sliding velocity	[m/s]
K	Thermal Diffusivity	[m^2/sec]
λ	Thermal conductivity	[W/m°C]
ρ	Density of the wheel	[kg/m^3]
C_p	Specific Heat capacity	[J/kg°C]
ß	Thermal penetration coefficient	[J/m^2°C$\sqrt{S}$]
$q_{friction}$	Frictional Heat flux	[W/m^2]
N_w	Normal load on a wheel	[N]
ε	Heat partitioning ratio	[-]
η	Equivalent material parameter	[1/MPa]
E	Modulus of Elasticity	[MPa]
N	Poisson's Ratio	[-]
k_{11}	Equivalent radius	[mm^{-1}]
k_{12}	Equivalent radius	[mm^{-1}]
k_{21}	Equivalent radius	[mm^{-1}]
k_{22}	Equivalent radius	[mm^{-1}]
Σk	Main equivalent radius	[mm^{-1}]
Ψ	Equivalent radius ratio	[-]
Po	The maximum contact pressure	[MPa]
$P_z(x,y)$	The normal pressure distribution	[MPa]
Ω	Reduction of the distance b/n wheel and rail centers	[mm]
n_a	Hertz parameter I	[-]
n_b	Hertz parameter II	[-]
M	Coefficient of Frictional	[-]
Φ	Angle of the contact planes	[°]
R_1	Rolling radius of the wheel side	[mm]
R_2	Longitudinal radius of the rail	[mm]
r_1	Wheel rolling radius	[mm]
r_2	Rolling radius of the rail	[mm]
T_{max}	Maximum surface temperature	[°C]
$ε_P$	Plastic strain	[mm]
$σ_y$	Yield strength	[MPa]
K_{Ic}	Fracture Toughness	[MPa$\sqrt{m}$]
G_{Ic}	Fracture energy	[N/mm]

Abrreviations

LEFM	Linear Elastic Fracture Mechanics
EPFM	Elastic Plastic Fracture Mechanics
XFEM	Extended Finite Element Method
GFEM	Generalized Finite Element Method
PUM	Partition of Unity Method
LRT	Light Rail Transit
FEM	Finite Element Method
FEA	Finite Element Analysis
HCT	Hertz Contact Theory
RCF	Rolling Contact Fatigue
RSA	Railway Safety Act
MAXPS	Maximum Principal stress Criterion
MAXPE	Maximum Principal strain Criterion
MAXS	Maximum nominal stress criterion
MAXE	Maximum nominal strain criterion
QUADS	Quadratic Nominal stress
QUADE	Quadratic Nominal strain
DOF	Degree of Freedom
SIF	Stress intensity factor
VCCT	Virtual Crack Closure Technique
PLM	Product Life cycle Management
PUFEM	Partition of Unity Finite Element Method
PEEQ	Equivalent Plastic strain
C3D8	An 8-node linear brick, full integration
C3D8R	An 8-node linear brick, reduced integration, hourglass control

DECLARATION

I hereby declare that the work which is being presented in this thesis entitled "**Simulation of crack propagation of a skidded rail wheel using Extended Finite Element Method (XFEM)**" is the original work of mine carried out under the supervision of Dr. Daniel Tilahun. The work contained in this thesis has not been previously submitted for a degree or Diploma at any higher educational institutions. To the best of my knowledge and belief, the thesis work contains no material previously published or written by another author except where due reference is made and all the resource papers used as an input had been accordingly acknowledged.

___Candidate_____ _____ _____

Natnael Mandefro Signature Date

This is to certify that the above declaration made by the candidate is correct to the best of my knowledge.

____Advisor_____ _____ _____

Dr. Daniel Tilahun Signature Date

ADDIS ABABA UNIVERSITY

ADDIS ABABA INSTITUTE OF TECHNOLOGY

SCHOOL OF MECHANICAL AND INDUSTRIAL ENGINEERING

Simulation of crack propagation of a skidded rail wheel using Extended Finite Element Method (XFEM)

By: NatnaelMandefro

Approved by board Of Examiners

Getasew Ashagrie	_____	_____
Acting Dean of SMIE	Signature	Date
Birhanu Beshah (Dr.)	_____	_____
Head, Railway Center	Signature	Date
Daniel Tilahun (Dr.)	_____	_____
Advisor	Signature	Date
Haileleoul Sahle	_____	_____
Internal Examiner	Signature	Date
Behailu Mamo	_____	_____
External Examiner	Signature	Date

Chapter One

Background and Justifications of the Study

1.1 Introduction

Transport is one of the key sectors that play crucial roles in achieving the goals of poverty eradication and sustainable development. The transport sector is very much linked and influence developments in other sectors of the economy.

Many of the world's large cities grew in conjunction with railways, and today, large cities cannot depend only on motor vehicles for transportation. With worries over global environmental issues, public transportation systems are increasingly seen as an important way to expand and revitalize large cities, while consuming less energy and other resources [1].

In Africa, road transport is the most dominant mode of motorized transport, accounting for 80% of the goods traffic and 90% of the passenger traffic on the continent. Road traffic accidents kill 1.2 million people in the world. Of this number, over 225,000, or 19%, were accounted for by deaths on African roads.

Railway transportation is relatively safer than road mode of transport so development of railway has a big advantage.

In 2005, the continent had a total railway network of 90,320 km or 3.1 km of per 1,000 km^2, most of which is disjointed. With the exception of North Africa, railways in Africa generally have a low level of traffic. The railways carry only 1% of the global railway passenger traffic and 2% of goods [2].

The specific characteristics of rail vehicles consist in the capability of travelling by means of wheels on the rails while ensuring also self-guidance through the contact forces between wheels and rails. Thus, wheels, besides the three features that are common for the majority of other terrestrial means of transport, i.e vehicles vertical support, running and propulsion, respectively braking, railway vehicles have an additional distinctive function, the self-guidance capability according to the distance between the two rails of the track.

As both wheels and rails are metallic, vehicles have the ability to carry loads far greater than other land transport systems. This skill, combined with that of self-guidance, generates the possibility of forming heavy convoys of vehicles (trains), which gives the wheel-rail system the advantage of a large transport capacity [3].

Railway transport is generally acknowledged for its low cost, environmental friendliness, energy efficiency, and fast speed (over short and medium distances) compared with other means of transportation. Of all the factors affecting railway operation, safety is the primary concern. For passengers and customers, accurate timetable, good ride comfort (for passengers), and low cost are also important. Therefore, railway operators and maintainers need to keep train service punctual, relatively quiet, comfortable, and low in cost to attract customers and compete with other means of transportation.

As an example, the railway system in China plays a demanding role among all of the methods of transportation (motor vehicle, ship, airplane, pipe line, etc). The cart wheel is one of the most critical components in the railway system. And it is proven that a wheel failure can cause a derailment with its attendant loss of life and property and should be considered effectively [4].

And also the railway track in Malaysia has shown the necessity of an efficient management of railway systems. The design is aimed toward reducing costs

and increasing safety, as well as reliability, of the railway systems. The wheel-rail interface is one of the most crucial points that must be checked to determine the performance of a train and consider its safety. And the damage in this area is due to repeated cyclic loading of the wheel [5]. Generic

1.2 Background of the Study

An analysis of data for Canadian railway accidents which occurred between 1999 and 2006 revealed that track and equipment factors dominate all other causes of mainline derailments. As illustrated in figure 1.1 below, track and equipment factors were identified in 63% of all main line derailments. Moreover, if one considers only those derailments where a contributing factor is cited (i.e excluding the 29% where a cause was not assigned), equipment and track factors accounted for 89% of all mainline derailments. Within the 34% of equipment related mainline derailments, wheel failures were the dominant cause [6].

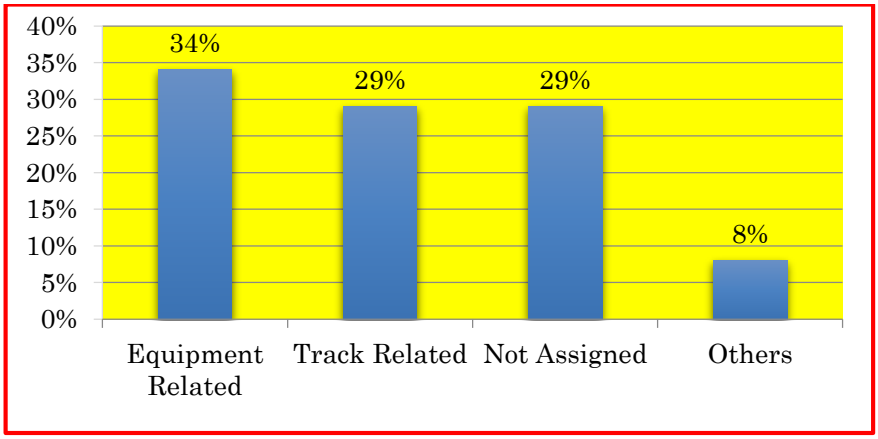

Figure 1.1: Canadian Mainline derailments by reported cause

Prediction of train accidents (abrupt failures) is critical for rational allocation of resources to reduce accident occurrence in the most cost effective manner possible. Train accidents cause damage to infrastructure and rolling stock as well as service disruptions, and may cause casualties and harm the environment. FRA of the U.S organized and categorized major train accident

cause from 2001-2010 as: Track, Equipment, Human factors, Signal and Miscellaneous [7]. Amongst the listed major cause of Train derailments according to FRA broken wheel is at the 4th list order out of 52.

And according to Yongming Liu et al [6] the proportional distribution of types of equipment failures on average over the interval 1999 to 2006 reported by CN and CPR (Canada's Class 1 Freight railways) and one can see that axles/wheels are the largest category in both cases see figure 1.2.

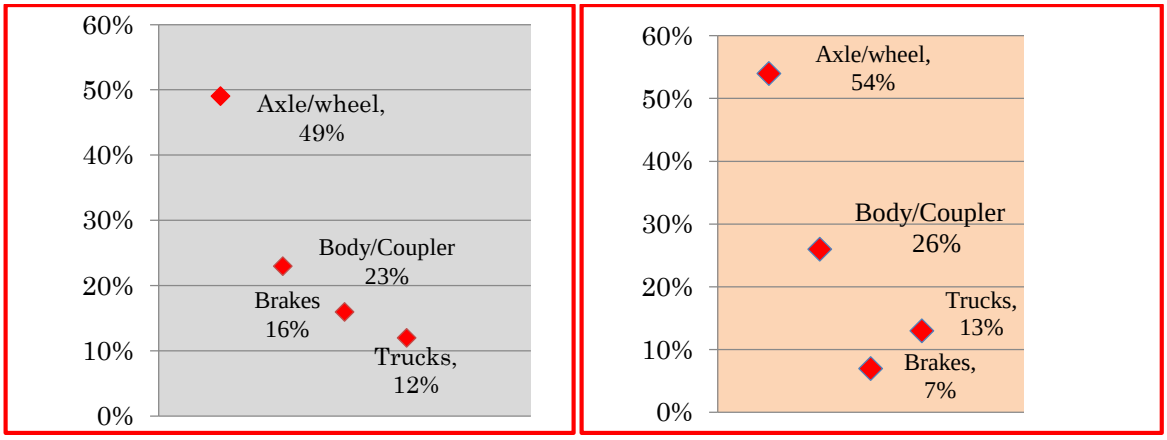

Figure 1.2: Major CN (Left hand side) and CNP (Right hand side) Derailments accident causes [6].

In June of 1998, one of Germany's Intercity Express (ICE) trains slammed in to an overpass, killing 101 people. The failure was traced back to a damaged wheel that disintegrated just before the train passed over a switch-track, causing cars to derail and impact the bridge's supports [8].

Different failure modes have been observed for railroad wheels, such as shattered rim, vertical split rim and thermal cracking. Shattered rim failures are the result of large subsurface cracks that propagate roughly parallel to the wheel tread surface. Thermal cracking usually breaks off a piece a piece of the wheel tread, while shattered rim can destroy the wheel's integrity and thus is more dangerous [6]. Surface induced fatigue failures stem from severe plastic deformation of the surface material. These failures are relatively harmless

(although costly) in that they normally result in the detachment of only a small part of the tread material. Subsurface failures, on the other hand, may result in the detachment of very large pieces of the rim material and even in a catastrophic failure of the entire wheel [9].

Subsurface cracks usually occurs at a depth 5-10 mm with 20^0 inclination [6] and [10].

The subsurface crack propagation rate depends on several parameters for every selected Fracture Mechanics approach such as Wheel Geometry (Diameter, rim thickness, and Plate Design), Loading conditions (Magnitude and Location), Residual stresses in the rim due to the manufacturing process and the thermal brake loading conditions, Wheel wear, and Subsurface crack attributes (Size, shape, and Orientation). Shattered rim and Vertical split rim crack growth rates depend on Crack size, Crack Orientation, Crack lateral location, and Crack vertical location below the tread surface [11].

Therefore, the failure of wheels is very costly in economic measures, it is very fatal in accident measures. Consequently it is an increasing need for predictive models and countermeasures to prevent such failures. These models presume an understanding of the underlying physical mechanisms. The propagation rate of defects is studied through a fracture mechanics analysis. Inspection intervals are then prescribed so that the defects will be detected before global failure occurs. Therefore, this thesis work aims at assessment of railway wheels safety in relation to the failure due to cracks by considering both thermal and static (mechanical) load using Extended FEM.

1.3 Statements of the Problem

Railway safety is the major issue for the transport service sector and for the well-being of the passenger also. Management of railway vehicle wheel sets accounts a significant proportion of rail vehicle maintenance activities and can be a key driver determining the vehicle or bogie maintenance periodicity [8]. Although wheel sets will have planned maintenance schedules, damage to the wheel surface may develop rapidly, requiring a wheel set to be taken out of service for repair or replacement at short notice. This can have an impact on a fleet's service provision as well as cost.

In the current Addis Ababa LRT project under ERC, the vehicles are equipped with Disc Braking system mounted on the axle. This system is a combination of mechanical devices operated by compressed air arranged in a system and controlled hydraulically by means of which the motion of cars and locomotives is retarded or stopped. When the air is released from the brake cylinder to push the brake caliper towards the brake disc then the train will retard or it will stop. If the returning spring attached to the piston that pushes the caliper towards the disk fails, the caliper will remain there holding the brake disc. Therefore, at the time of train movement the wheel set that encountered such failure (Jamming/locking) will not have a rotational motion rather it will slide along the rail during the entire journey.

Skating is when the ratio of the Normal force and the brake torque is about 2 and skating the wheel on the rail therefore will induce a high frictional heating temperature that greatly affect the sub-surface defects to propagate than micro-sliding between wheel/rail.

Fully functional brake systems are not likely to induce thermal crack propagation under normal stop braking, but that with pre-existing defects a severe drag braking due to malfunctioning brakes may cause very deep

cracking [12]. The combination of thermal and mechanical fatigue on the wheel can greatly contribute to the propagation of crack on the tread surface [16].

Most researchers go through crack initiation and propagation analysis of railway wheels due to different loading conditions. Some of them focus only on mechanical stresses that can cause crack to propagate and the rest considered thermal stresses crack loading induced during braking, slippage of the wheel or due to the skating of the wheel due to jamming of brakes. Few of the researchers considered both of the loading conditions assuming a faster crack propagation rate. Most of the FEM approach they used needs a concern in that for every crack length there is a need of re-meshing

This thesis work aimed at filling the gap of considering cracks induced from larger sliding velocity due to the brake jamming and static mechanical contact pressure by utilizing an efficient mathematical formulation found in ABAQUS known as extended finite element method (XFEM).

Therefore, this phenomenon highly pushes this thesis work towards examining the subsurface crack propagation under **malfunctioning of Brake** using selected parameters for sensitivity study.

1.4 Objectives of the Study

1.4.1 General Objectives

The main objective of this study is to make an analysis on the crack propagation related schemes of Railway wheels under Thermal and Mechanical loads in Malfunctioning (Jamming) of Disc Braking systems.

1.4.2 Specific Objectives

This study specifically aims at:

1. Determine the dimensions of the Elliptical contact patch minor and major axis lengths?.
2. Calculate the pressure distribution along the Elliptical contact patch?.
3. Simplify the elliptical contact to an equivalent rectangular area of contact?.
4. Determine the induced thermal stress and temperature due to the frictional heating during the skidding of the wheel?.
5. Checking the initial crack propagation scheme due to the contact pressure only i.e compressive loading.
6. Simulate the subsurface and surface cracks propagation due to the combined contact pressure and the induced frictional heat flux.
7. Provide appropriate result discussion and conclusion to meet the major objective of the study.

1.5 Significance of the Study

The Author strongly believe that this thesis has the following prominent values

- The analysis steps and the modeling used in this paper are synergistically generated from different fields of science like Contact mechanics, Thermal and Fracture Mechanics sciences for railway application and have its own credit in idea generation in Modeling Fracture problems in relation to wheel/Rail contact phenomena.

- The finding of this research will serve as input to a more deep and advanced studies in the future.
- The finding and the steps are helpful for safety periodic assessment and regulation need at glance for maintaining safe working cost for any railway companies.

1.6 Scope of the Study

The study focuses on

- Checking the degree of severity of wheel lock-up in crack propagation of a railway wheel.
- Modeling the wheel/rail contact under simplified hertz contact theory based on efficient assumptions stated.
- Estimating the frictional heat generated due to skidding of the wheel based on simplified assumptions like no heat transfer to the surrounding air.
- Employment of Extended Finite Element (XFEM) based on the Cohesive segment approach for Elastic-Plastic (non-linear) material type and for Edge crack (surface crack) and Horizontal crack (Subsurface crack) at different initial length of the artificial cracks insertion on a simplified wheel geometry using ABAQUS commercial software.
- Generating results by with regard to crack tip maximum principal stress and Plastic strain with slightly increasing crack length, Δa to have a clear insight about the crack propagation scheme.

1.7 Research design and Methodologies

1. Research Design

The research addresses the crack propagation analysis of a railway wheel under thermo-mechanical stresses induced during jamming of brakes and wheel skating. A comparative investigation of the Addis Ababa LRT braking systems and overall operation is assessed. Examining and adopting theories and modeling approaches regarding the complex wheel/rail contact geometry

prediction, frictional heating load and FE based fracture mechanics application to the railway science specifically for Elastic-plastic materials were done. Based on the maximum severe case scenario and simplicity, better modeling approach for the study is selected. The model selected can clearly ease thermo-mechanical wheel cracking assessment for a general purpose of railway systems.

Finally, based on the basic data collected to simulate the problem efficient simulation techniques were applied to get accurate result as much as possible on the analysis software. To compare the normal and severe operating conditions, two different loading conditions were considered i.e pure contact pressure and sequentially coupled thermal and mechanical load. As a sensitivity study, crack orientation angle, different initial crack lengths were investigated along with subsurface and surface crack comparison for both loading cases. The overall approach of the study is mapped in the research framework section 3.2 and illustrated using diagram in Figure 3.1.

2. Research Framework

The research framework of the thesis is designed based on the existing concepts in railway science and fracture mechanics fields of studies. The assumptions considered in designing the research frame work are listed below

1. The wheel set is moving at the center of the intersection between wheel contact and rail contact geometry (No lateral movement of the wheel set).
2. There is Equal load distribution for each wheel fitted to the Bogie.
3. The contact patch pressure is constant through time and doesn't change with temperature.
4. Coulomb's friction law is applicable between wheel and rail contact.
5. No Residual stresses during manufacturing that could be considered in the Analysis.

6. No Residual stresses remain in the wheel due to shrink fitting of the wheel on the axle.
7. Cracks or flaws do exist in the wheel.
8. Using the average pressure than the elliptical contact pressure distribution has equivalent effect.
9. The surface of the rail has no irregularities and corrugation so it is rectilinear and stable ride.
10. The wheel is fitted with the axle firmly so that there is no relative movement or slippage.
11. All the frictional heat induced is partitioned to the wheel.

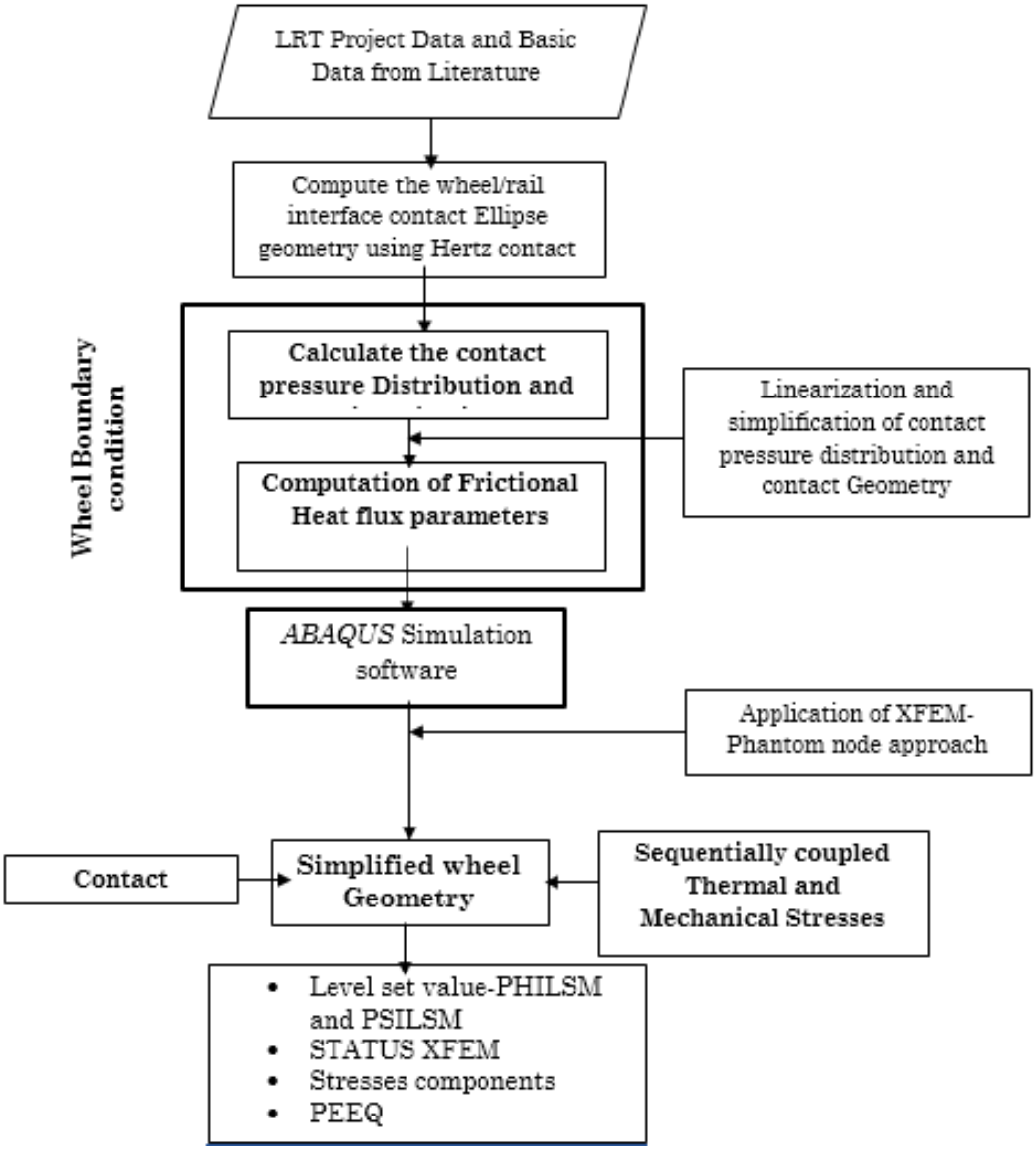

Figure 1.3: Research framework Design

3. Research Methodologies

The research methodologies employed different approaches to achieve its objectives. The following methodologies are used to secure both qualitative and quantitative and secondary data. Necessary data are then either collected or simulated depending on their availability. This may include data from the already existed data. The different methodologies used in the thesis are explained below.

3.1 Literature Review

In the literature review, different articles, periodicals, thesis, dissertations, books, websites, and other materials were surveyed in order to meet the listed objectives. The literature review examined different working models of calculating wheel-rail contact patch geometry dimensions, predicting heat generated due to wheel sliding, fracture of wheels and the application of the extended finite Element Method (XFEM) were surveyed so as to isolate the appropriate problem modeling technique.

3.2 Secondary Data

In order to adopt the study to the current LRT project of Ethiopia, the easiest way is to collect operating parameters of the E-W route of the LRT project data. The variables needed include.

1. The maximum carrying capacity of the train.
2. The average distance between two stations.
3. The maximum operating speed, acceleration and deceleration of the train.
4. Number of axles and wheels per vehicle.
5. The geometry of the wheel and rail and their dimension.

4. Tools and Methods

The computer aided design software called PRO/Engineer was used to draw the full wheel model. MS-Excel and MatLab R2012a softwares are used to handle the mathematical manipulations and plotting graphs in the analysis step. Abaqus simulia 6.12.1 software package was used as a main crack propagation analysis software.

The Methods used in this thesis are: Hertz contact theory approach for determination of the elliptical contact dimension and pressure distribution

calculation, Extended Finite Element Method (XFEM) which is an extension of the classical finite element method which has the capability of simulating problems with discontinuities and real life proofed crack initiation and propagation capability.

1.8 Limitations of the Study

The limitations of the study are

- Difficulty of modeling the wheel under dynamic running conditions considering every component of the car force components imposed on it.
- Some assumptions taken may have negative effect as compared to the actual operating conditions.
- Deficiency of material properties for distinct material type selected.

1.9 Organization of the Study

The thesis is organized in six chapters.

Chapter One is the introductory part which clearly states the Background information, Statement of the Problem, Major and specific objective, Major research questions, Significance of the study, Scope of the study, Limitation of the study, and Organization of the paper.

Chapter Two is the Literature review. In this section, enough coverage of articles and papers are reviewed in Contact mechanics science, Frictional heat phenomenon and Fracture mechanics and XFEM analysis and related papers are reviewed regarding their area of coverage and their gaps.

Chapter Three is Research method and Numerical Framework. It describes the flow of the study with their general numerical and analytical frame works.

Chapter Four is about Analysis and Modeling. Numerical parameter calculations manual and using MATLab R2012a is presented. Modeling in

Extended Finite Element analysis (XFEM) routine of ABAQUS software and steps are described.

Chapter Five is for Result and Discussion. In this section the results obtained from the ABAQUS software are presented and Discussed as per the objective set.

Lastly, Chapter Six cover the Conclusion, Recommendation and Future research directions. In this chapter Conclusion are drawn based on the results discussed in chapter five for the different parameters selected, based on the concluded remarks some points are recommended and finally the future works as an extension to this study are outlined.

Chapter Two

Literature Review

2.1 Wheel Damages

In fact, RCF cracks are one of the most important problems for the railway industry [7]. It is also presented by researchers that the major wheel damage is shifted from wear to Rolling contact fatigue since wear cause slow deterioration of wheels whereas fatigue causes abrupt fractures in wheels or the tread surface material loss [6].

But in general, the overall incidence of wheel damage from the observation from a sample set of vehicles was presented below.

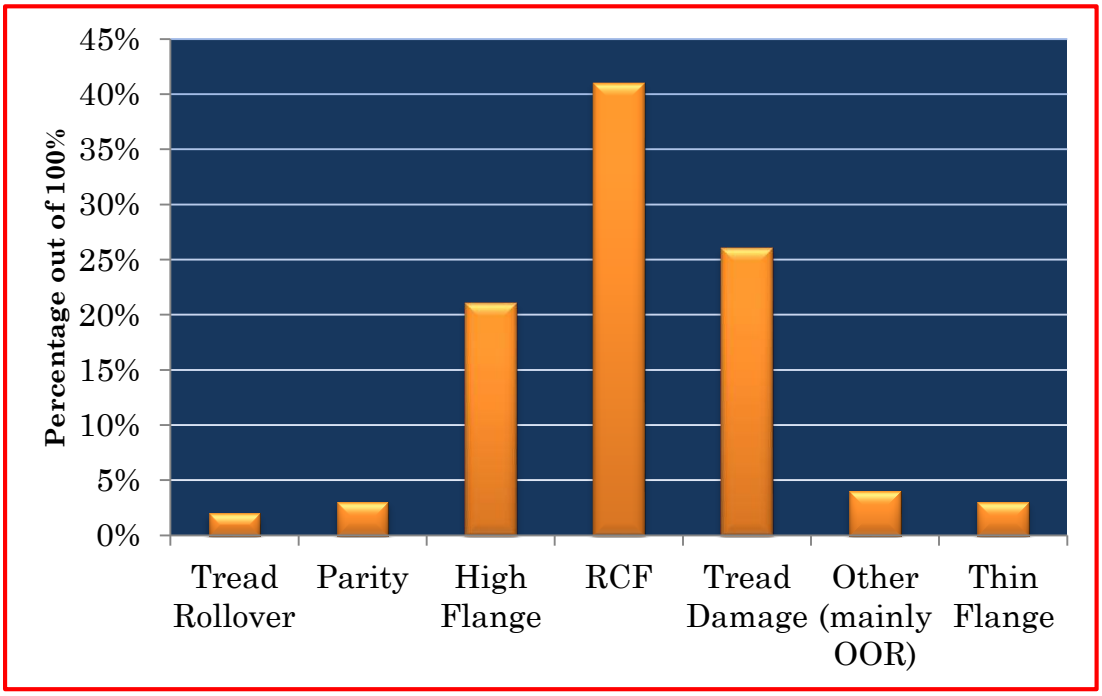

Figure 2.1: Overall incidence of wheel damage (Adopted from [8])

Table 2.1: Wheel failure mechanisms [8].

No	Damage Type	Cause
1	Rolling contact Fatigue (RCF)	Due to Fatigue-related damage that is induced as a result of the repeated cyclic loading and unloading together with the additional creep forces from curving, traction and braking.
2	Thin flange	Wear on the face of the wheel flange.
3	High Flange	Wear concentrated across the flange of the wheel.
4	Tread damage	A combination of wheel material defect, wheel spin or slide,
5	Tread rollover	Deformation of the tread material causing a lip to develop in place of the chamfer on the field side of the wheel.
6	Parity	Turning of wheels on a wheel lathe.
7	Other	Includes wheels turned for reasons other than the damage mechanisms listed above. This includes Out-off round wheels due to wheel machining issues or the presence of other tread damage and observations of poor ride or vehicle stability issues.

And for most of wheel failures due to fracture crack propagation into the wheels inner surface plays a major role. Based on the study from observation, the failure mechanism due to crack of the wheels is divided in to three categories[13]:

A. Superficial cracks

This type of cracks usually occurs because of severe plastic deformation which is a result of contact stresses. Deformations can occur because of excessive loading (more than the designed limit). Wheel failure including spalling, shelling, severe deformation and etc. are all of this type of failure. This type of fatigue is of low cycle.

B. Under surface cracks

These cracks are produced because of under surface stresses. Fatigue cracks usually start from some millimeters under the wheel surface where maximum shear stress occurs. Wheel failures which are namely called deep shelling and shattered rim are of this type of failures. This type of fatigue is of long life cycle.

C. Under surface cracks with a high depth

Such cracks usually occur because of material impurities during production process.

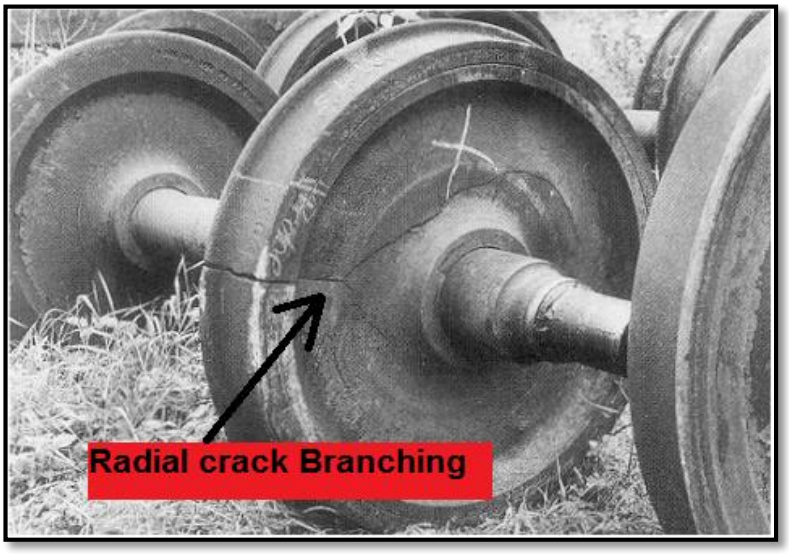

Figure 2.2: Wheel failure due to crack

Fatigue in wheels is concerned with rolling contact fatigue which is produced during rolling movement under the effect of alternative contact stresses [2].

RCF can be observed as a characteristics regularly spaced crack pattern all around the circumference of the wheel. This damage type is one of the common types of fatigue damage in railway wheels, related to excessive plastic straining of the material in the surface [3].

Wheel Damage causes

The major causes of Wheel damages in relation to the load can be broadly categorized in to:

1. **Mechanical loads**

   Mechanical load in most general perspective is the load without thermal load (frictional heat) including static axle load, lateral force, dynamic loads, and tractive force [66]. The contact area between a train wheel and rail has barely the size of a thumbnail. Stresses in this area are amongst the highest known in engineering, even if only the mechanical load due to the axle static load and tractive forces is considered [4] and [15]

2. **Thermal load**

   Thermal input in a wheel with disc brakes typically arises from forces during curve taking, wheel lockup, hunting oscillation etc. If these effects are large, extensive slip, i.e creep between wheel and rail may take place and heat can be generated due to friction and plastic deformation [3]. Sliding friction between railway wheels and rails results in considerable contact temperatures and gives rise to severe thermal stresses at the surfaces of the wheels and rails [4].

Figure 2.3: Fatigue crack on the Tread propagated from thermal crack

On account of this, the effect of the two loads surely cause considerably high wheel damage due to crack propagation and wear [11][12][17].

2.2 Wheel-Rail Contact

Wheel-rail contact geometry prediction is the most unsaturated research area in railway engineering and is considered complicated due to the elastic deforming and the contact profiles. Finding the contact area and pressure distribution requires complex programming and long computational time.

2.2.1 Hertz Contact Theory (HCT) Model

The first satisfactory analysis of the stresses at the contact of two elastic solids was developed by Hertz according to [18][19] based on the theory of elasticity. For normally loaded contacts, the best-known analytical method is the Hertzian theory established by Hertz in 1882. Hertz model of contact stress relies on the following simplifying assumptions

1. The materials in contact are homogeneous and the yield stress is not exceeded.
2. Contact stress is caused by the load which is normal to the contact tangent plane, which implies that there are no tangential forces acting between the solids.
3. The contact area is very small compared with the dimensions of the contacting solids. (The half space assumption puts geometrically limitations on the contact, i.e., the significant dimensions of the contact area must be small compared with the relative radii of the curvature of each body [20] .
4. The surface slopes are so small that all pressure (Normal tractions) can be considered to act in the direction parallel to the direction of loading.
5. The contacting solids are at rest and in equilibrium.
6. The effect of surface roughness is negligible.

The configuration of two elastic bodies with convex surfaces in contact is the basis of Hertz's theory [20] .

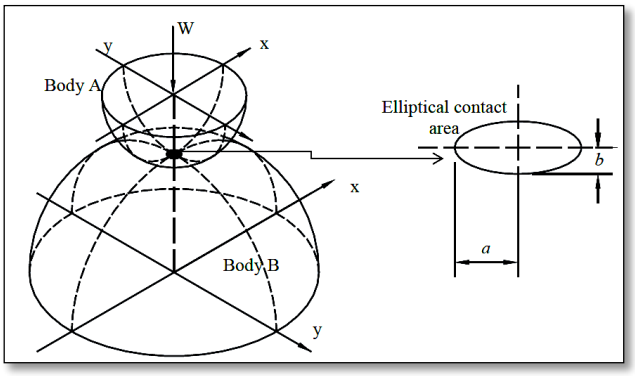

Figure 2.4: Geometry of two elastic bodies with convex surfaces in contact [20].

The size and shape of the contact zone where the railway wheel meets the rail can be calculated with different techniques. The half space assumption puts geometrically limitations on the contact, i.e., the significant dimensions of the contact area must be small compared with the relative radii of the curvature of each body [21].

The HCT leads to an elliptical contact area and a semi-ellipsoid contact pressure distribution in the contact region. Due to its efficiency and simplicity this model has been extensively applied [22].

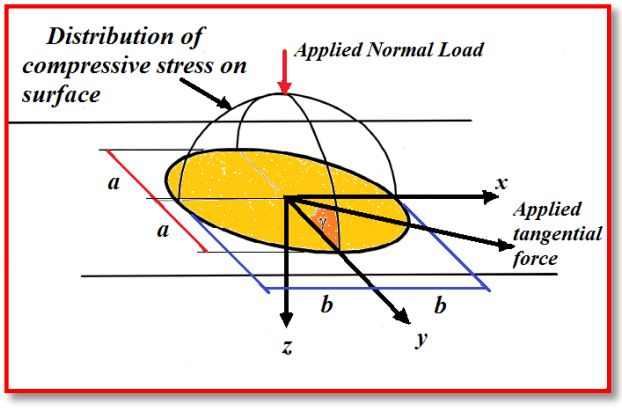

Figure 2.5: Loads on an Elliptical Hertzian contact patch [23].

For elliptical Hertzian contact, the contact pressure is given by,

$$P_z(x,y)=P_o\sqrt{\left(1-\frac{x^2}{a^2}-\frac{y^2}{b^2}\right)} \quad \text{.....Eq 2.1}$$

Where P(x,y) is the contact pressure, p_o is the maximum contact pressure at the first point of contact, while a and b are the lateral and longitudinal semi-axes of the contact ellipse, respectively.

$$P_o = \frac{3N}{2\pi ab} \quad \text{.....Eq 2.2}$$

The easy way of finding the contact parameters is discussed in [14] [20], the equations of the parameters are:

Where the η parameter and the equivalent radii are as follows:

$$k_{11} = \frac{1}{R_1} \quad \text{.....Eq 2.3}$$

$$k_{12} = \frac{1}{r_1} \quad \text{.....Eq 2.4}$$

According to [64], the Equivalent radius k_{12} can be determined from

$$X = \frac{3.358537058}{100}Z + \frac{1.565681624}{1000}Z^2 \quad \frac{2.810427944}{100000}Z^3 + \frac{5.844240864}{10^8}Z^4$$
$$\frac{1.562379023}{10^8}Z^5 + \frac{5.309217349}{10^{15}}Z^6 \quad \frac{5.957839843}{10^{12}}Z^7 + \frac{2.646656573}{10^{13}}Z^8 \quad \text{.....Eq 2.5}$$

Thus, wheel curve in the point contact with rail is calculated as the following:

$$k_{12} = \frac{|X''|}{(1+X'^2)^{3/2}} \quad \text{.....Eq 2.6}$$

$$k_{21} = \frac{1}{R_2} \quad \text{.....Eq 2.7}$$

$$k_{22} = \frac{1}{r_2} \quad \text{.....Eq 2.8}$$

$$\sum k = k_{11} + k_{12} + k_{21} + k_{22} \quad \text{.....Eq 2.9}$$

The Equivalent ratio (Ψ) is used to find the coefficients n_a, n_b and n_δ and is given by:

$$\Psi = \frac{1}{\sum k}\sqrt{(k_{11}-k_{12})^2 + (k_{21}-k_{22})^2 + 2.(k_{11}-k_{12}).(k_{21}-k_{22}).\cos 2} \quad \text{...Eq 2.10}$$

The geometrical quantities used in the analytical computation can be seen below in the figure:

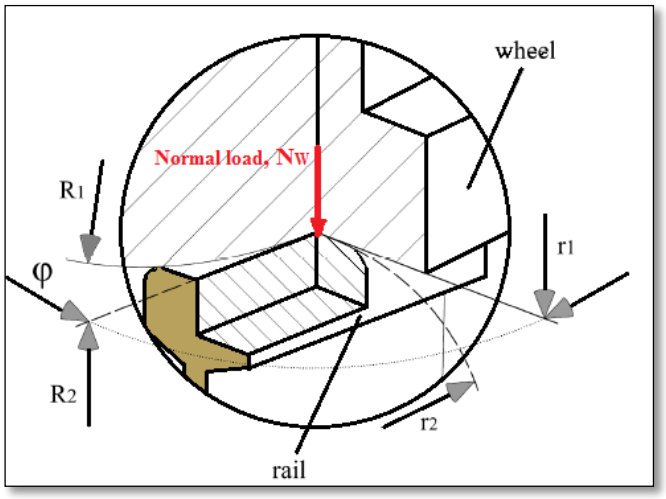

Figure 2.6: Application of Hertz theory for Wheel/Rail contact

The length of the semi axis of the contact ellipse a and b is therefore:

$$a = n_a \sqrt[3]{1.5N_w \frac{\eta}{\sum k}} \quad \text{.....Eq 2.11}$$

$$b = n_b \sqrt[3]{1.5N_w \frac{\eta}{\sum k}} \quad \text{.....Eq 2.12}$$

2.2.2 Non-Hertzian Contact Model

Paul and Hashemi were the first to publish a non-Hertizian contact problem solution [58]. Several investigations show that the contact patch has non-elliptic shape even wheel tread-rail head contact. This is because the contact patch in this case is spread widely in the lateral direction and thus the relative lateral curvature is varied through the patch.

A. The Equivalent Ellipse

To simplify the contact area even more, Pascal and Sauvage [26], used a method to calculate only one equivalent contact ellipse at the wheel set central position by which the ratio of the equivalent ellipse is the weighted mean of the ratios of the two ellipses which approximates the real contact.

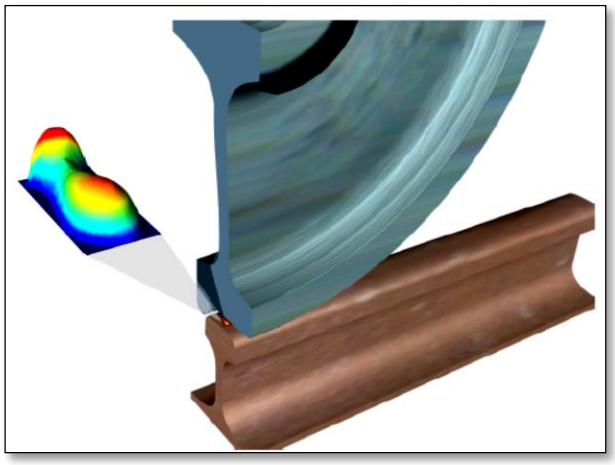

Figure 2.7: Exemplary contact patch between wheel and rail [26]

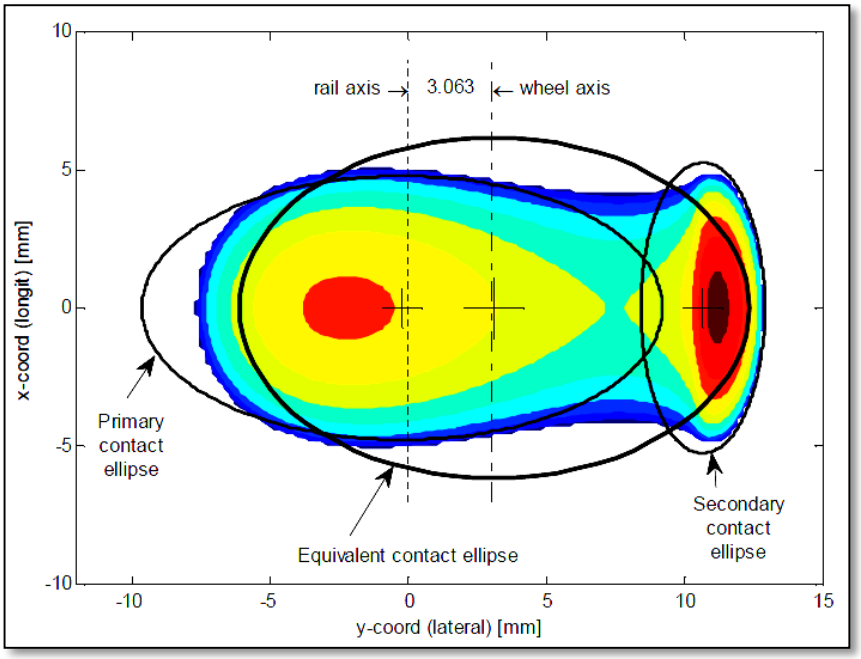

Figure 2.8: Equivalent ellipse for the wheel-set positioned in the center of the track [24]

According to [24], equivalent elliptical contact gives a good approximation for the real case, as long as no flange contact occurs between wheel and rail.

B. Other Advanced Contact Models

In addition to the traditional Hertz contact which assumes linear-elastic frictionless contact between the contacting surfaces, two other methods been

used to investigate wheel-rail contacts, namely Kalker's two software programs CONTACT and FASTSIM.

Kalker's CONTACT software divides the three dimensional non-elliptical contact zones into cells and uses a boundary element analysis with a half-space assumption and a linear material model to solve the contact problem. In FASTSIM, the normal problem is solved using the Hertz analytical method and the tangential problem using a modified Winkler elastic foundation model. This approach increases the calculation speed as compared to the CONTACT program. [56]

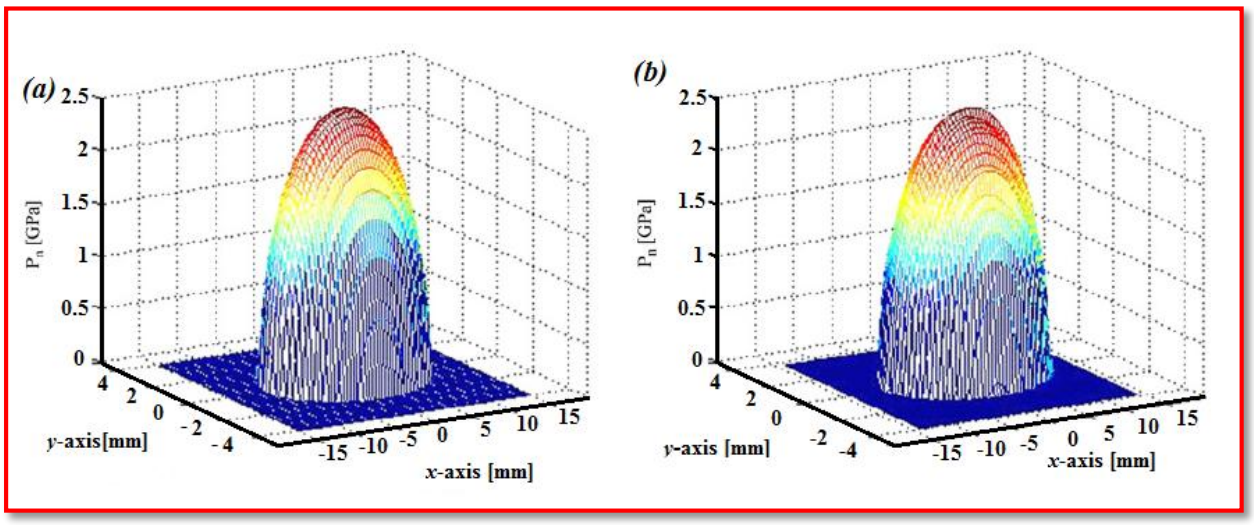

Figure 2.9: Contact Pressure Distribution using (a) Hertz method (b) Kalker's Contact Software

2.2.3 Wheel-Rail Sliding

The phenomenon where among the two meting (contacting) surfaces move over the other in continuous contact with smooth or slippery medium of contact is called Sliding or skidding. At sliding high temperatures occur which may cause plastification and material transformation followed by the buildup of a zone in the wheel tread with residual stresses and Martensite [25].

Wheel-Rail Friction Models in Dry Condition

Accurate estimation of wheel-rail friction levels is of extreme importance in train simulations. The software programs for vehicle dynamic simulations use built-in friction data based on optimum conditions, i.e the tracks are dry, so the train makes use of its maximum power during acceleration. Friction in dry contacts takes place at micro level and is generated in the micro-contacts of surface roughness.

According to [18] we have three contact regions and states that Region B is more severe (see figure 2.10), having higher contact stresses and wear rate than that of the two regions.

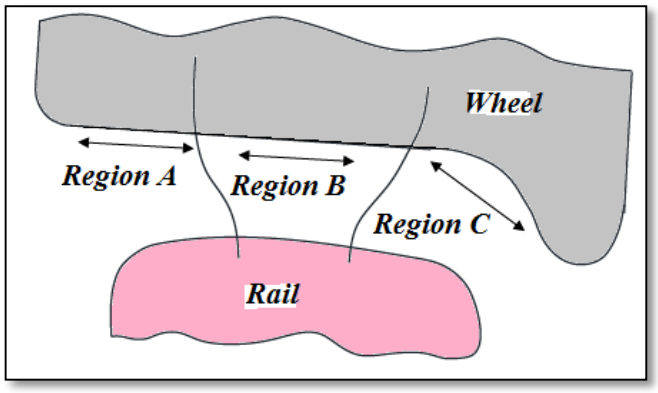

Figure 2.10: Rail-Wheel contact zones [18].

2.3 Frictional Heating Phenomenon

Frictional heating during braking, Jamming of brakes (wheel skidding) and also in macro-sliding phenomenon is a very important research field of railway technology. There are several publications that discussed about the heat generation, temperature and stress distribution because of sliding bodies i.e moving heat sources.

The first investigation on flash temperature investigation was conducted by Harmen Blok [27] in 1937. He examined and defined for a semi-infinite body,

using a uniform square heat source i.e the maximum surface temperature rise at different (low and high) Peclet numbers. J.C.Jaeger [28] in 1942 also made an attempt in connection with the problem of plane sliding to set out fully the assumptions made and the numerical consequences of the mathematical theory to discuss particular models of sliding. J.R. Barber [29] in 1967 tries to find a derived solution for the heat conduction in a single interaction i.e the mechanism of sliding for a single asperity interaction for a short duration. In 1984, B.A. Sherwood and W.H. Bernard[30] tries to find a solution for a model-independent work and heat transfer in the presence of sliding motion.

Heat and Temperature in Wheel-Rail Contact Patch Area

K.Knothe and S.Liebelt [31] tries to determine the temperatures for sliding contact for wheel-rail systems by applying Laplace transforms and Green's functions method. They investigated the distribution of Temperature due to surface roughness and indents. V.Gupta et al [32] tries to formulate 3D and 2D FEA of friction heat with time of a wheel attending rolling plus sliding by varying different combination of creep and adhesion. F.D. Fischer et al [33] analyzed thermal stress fields for frictional contact in wheel-rail systems and the results are given in dimensionless form. Martin Ertz and Klaus Knothe [34] go through a more detailed investigation to find a semi-analytical and numerical methods other than Blok's flash temperature formula. The same authors [35] find out an approximate analytical solution of the thermal stresses and shakedown in wheel/rail contact for a line wheel/rail contact model. There is a different temperature distribution scheme for every contact patch distribution.

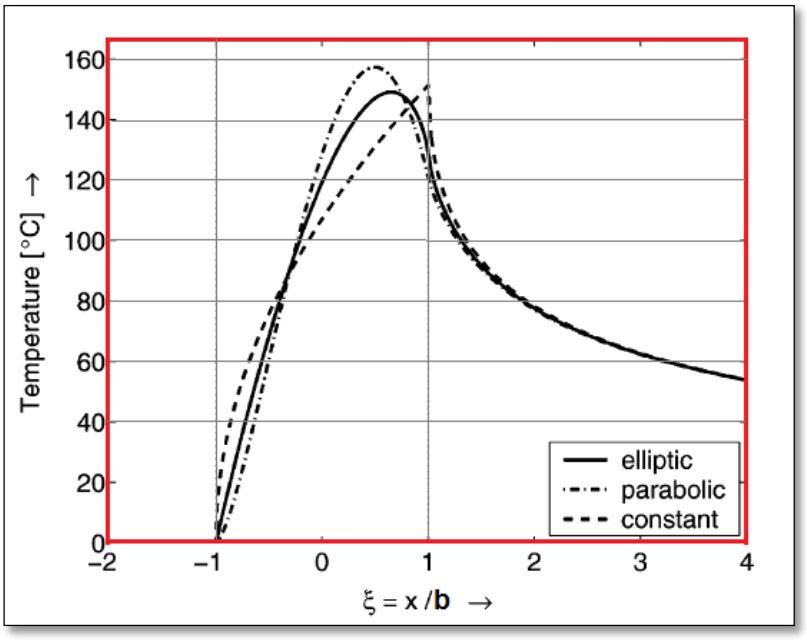

Figure 2.11: Surface temperature for various distributions of frictional heat flows

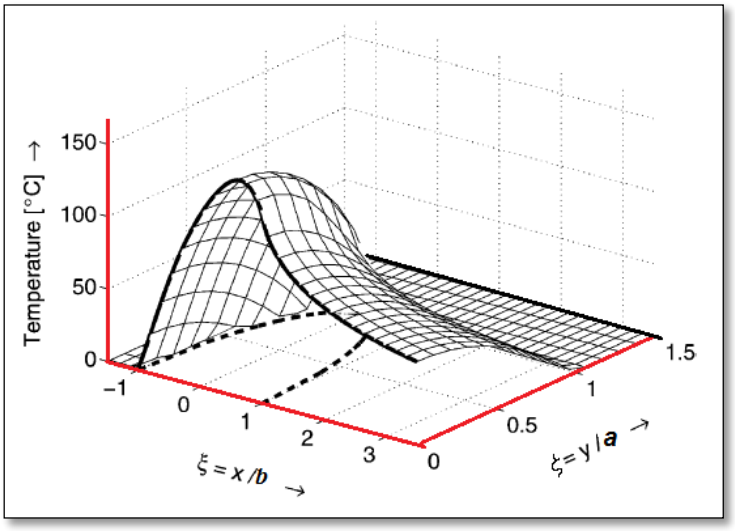

Figure 2.12: Surface temperature for Elliptical area of contact [35]

F.D.Fischer et al [33] try to find the analytical solution for frictional heat distribution over the wheel in dimensionless form depending on two parameters dimensionless thermal penetration depth and poisson's ratio. M.Ertz and K.Knothe [14] finds an easy and accurate way of finding a solution for frictional

heating in wheel/rail contact having constant heat flow rate which conformed to all the theories developed earlier as follows

If a tangential force T is transmitted between wheel and rail, there is always a mean relative velocity in the contact point. High contact temperatures are to be expected only with the transmission of tractive or braking forces at high relative velocities. In this situation, sliding occurs within the whole area of contact and the tangential force is T=μN. The coefficient of friction μ is assumed to be constant.

The contact patch moves with respect to the wheel surface and the frictional heating within the contact patch is a time-dependent heat source and during the very short period of time the penetration depth is very small as compared with that of the size of the contact patch. That is

$$\delta = \frac{a}{\sqrt{L}} \quad \text{.....Eq 2.13}$$

And it depends on the non-dimensional Péclet number, which can be defined as the ratio of the surface speed to the rate of diffusion of heat in to the solid

$$L = \frac{aV_s}{2k} \quad \text{.....Eq 2.14}$$

With the semi axis length $\boldsymbol{a}$, the speed $\boldsymbol{v}$ of the moving heat source and the thermal diffusivity, k which can be written as

$$k = \frac{\lambda}{\rho c} \quad \text{.....Eq 2.15}$$

where λ is the Thermal conductivity, ρ is the density and c is the specific heat capacity.

And the Thermal penetration coefficient,

$$\beta = \sqrt{\lambda \rho c} = \frac{\lambda}{\sqrt{k}} \quad \text{.....Eq 2.16}$$

With constant values of the coefficient of friction μ and the sliding velocity V_s the frictional power dissipation rate in the contact patch is proportional to the pressure:

$$\dot{q}_{friction}(\xi) = \mu . V_s . P_Z(\xi) = \mu . V_s . P_o \sqrt{1 - \xi^2} \quad \text{.....Eq 2.17}$$

It is generally assumed that all the frictional power dissipation is transformed in heat. The heat generated in the contact patch flows into the material of wheel and rail. With the heat partitioning factor ε, this can be written as

$$\dot{q}_w(\xi) = \varepsilon . \dot{q}_{friction}(\xi) = (1 - \varepsilon) . \dot{q}_{friction}(\xi) \quad \text{.....Eq 2.18}$$

The surface temperatures of wheel and rail must be equal everywhere in the contact patch. The heat partitioning parameter based on the duration of sliding time and sliding velocity is given in [37].

$$\varepsilon(t) = \frac{t^{0.5}}{t^{0.5} + 0.863\left(\frac{b}{V_S}\right)^{0.5}} \quad \text{.....Eq 2.19}$$

2.4 Fracture Mechanics

Fracture is a problem that society has faced for as long as there have been man-made structures. The cause of most structural failures generally falls into one of the following categories: Negligence during design, construction, or operation of the structures and application of a new design or material, which produces an undesirable result[38].

Fracture Mechanics is field of solid mechanics that deals with the mechanical behavior of cracked bodies[39]. And Crack is a type of fracture that separates a

solid body in to two, or more, pieces under the action of stress in three major modes: Mode I, Mode II, Mode III or a combination of one and the other[40].

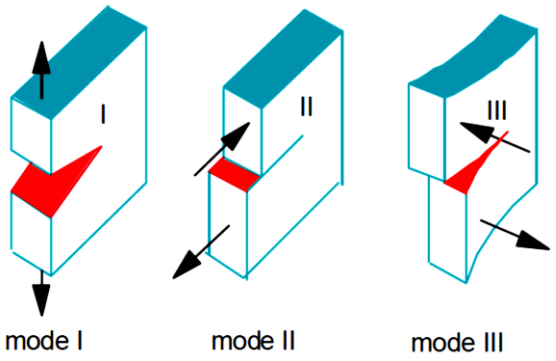

Figure 2.13: The three loadings of crack: a. Tension b. Shear c. Tearing [40]

For linear elastic Materials, Griffith's approach says that a crack extends if the thermodynamic crack driving force, characterized by the energy release rate *G*, becomes equal or larger than the crack growth resistance, R (Griffith, 1921) [38][41] where as in 1956 Irwin proposed an energy approach for fracture that is essentially equivalent to the Griffith model, except that Irwin's approach is in a form that is more convenient for solving engineering problems. He postulates that a crack grows when the crack tip stress intensity factor *K* reaches a critical value K_c.

The Griffith and Irwin criteria are equivalent for linear elastic materials, since energy release rate and stress intensity factor are related. The assumptions taken in LEFM analysis is listed below [38]:

1. A sharp crack or flaw of similar nature already exists; the analysis deals with the propagation of the crack from the early stages.
2. The material is linearly elastic.
3. The material is Isotropic.
4. The size of the plastic zone near the crack-tip is small compared to the dimensions of the crack.

5. The analysis is applicable to near-tip region.

Linear Elastic fracture mechanics (LEFM) is valid only as long as non-linear material nonlinear material deformation is confined to a small region surrounding the crack tip. In many materials, it is virtually impossible to characterize the fracture behavior with LEFM, and an alternative fracture mechanics model is required.

Elastic-Plastic Fracture Mechanics applies to materials that exhibit time dependent, nonlinear behavior (i.e plastic deformation) [41]. For crack growth in elastic-plastic materials under large scale or general yielding conditions, the common approach is to use criteria based on the crack tip opening displacement (CTOD) by Wells in 1963, Rice's J-integral in 1968 [38] and the energy dissipation rate by Turner and also Turner Kolednik in 1994.

2.5 Extended Finite Element Method (XFEM)

The standard finite element method (FEM) provides substantial advantages in dealing with continuous field problems. However, for discontinuous field problems, it is computationally expensive to obtain to obtain accurate solutions with polynomial approximations. Alignment of mesh with discontinuity becomes a major difficulty when treating problems with evolving discontinuities where the mesh must be regenerated at each step, i.e re-meshing is needed continuously [42]. Modeling of cracks in structures and specially involving cracks requires the FEM mesh to conform the geometry of the crack and hence needs to be updated each time as the crack grows. This not only computationally costly and cumbersome but also results in loss of accuracy as the data is mapped from old mesh to the new mesh [43].

A re-meshing technique is traditionally used for modeling cracks within the frame work of finite element method where a re-meshing is done near the crack to align the element edges with the crack faces [43].

The Extended finite element method (XFEM), also known as generalized finite element method (GFEM) or Partition of unity method (PUM) is a numerical technique that extends the classical finite element method (FEM) approach by extending the solution space for solutions to different equations with discontinues functions. It was first introduced by Bolyteschko and Black[45].
The extended finite element method (XFEM) has proved to be a competent mathematical tool [46] since it is an extension of partition of unity; allows the presence of discontinuities in an element by enriching degrees of freedom with special displacement functions. [47]

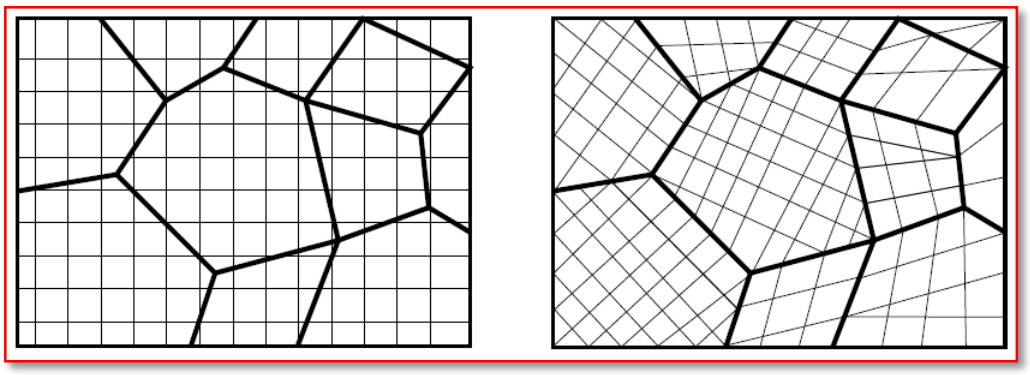

Figure 2.14: Mesh discretization in XFEM (left) and FEM (right)[48].

In comparison to the classical finite element method, the XFEM provides significant benefits in the numerical modeling of crack propagation. The traditional formulation of the FEM, the existence of crack is modeled by requiring the crack to follow element edges. In contrast, the crack geometry in the XFEM need not to be aligned with the element edges, which provides flexibility and versatility in modeling.

The Extended Finite Element Method (XFEM) can dramatically simplify the solution of many problems in material modeling such as the propagation of cracks, the evolution of dislocations, the modeling of grain boundaries and the evolution of phase boundaries [48].

The method is based on enrollment of the FE model with additional degrees of freedom (DOF) that are tied to the nodes of the elements intersected by the crack [49][50]. In this manner, the discontinuity is included in the numerical model without modifying the discretization, as the mesh is generated without taking into account the presence of the crack. Therefore, only a single mesh is needed for any crack length and orientation. In addition, nodes surrounding the crack tip are enriched with DOFs associated with functions that reproduce the asymptotic LEFM fields. This enables the modeling of the crack discontinuity with in the crack tip and substantially increases the accuracy in the computation of the stress intensity factors (SIFs).

2.5.1 Partition of Unity Finite Element Method, PUFEM

Partition of unity is a set R of continuous functions from X to the interval [0, 1] such that for every point, $x \in X$,

- There is a neighborhood of x where all but one finite number of the functions of Rare 0,
- The sum of all the function values at x is 1, $\sum_{i=1}^{n} f_i(x) = 1$

Partitions of unity are useful because they often allow extending local constructions to the whole space. They are also important in the interpolation of data, in signal processing, and the theory of spline functions [50].

To improve a finite element approximation, the enrichment procedure may be applied. In other words, the accuracy of solution can be improved by including the analytical solution of the problem in the finite element formulation. In fracture mechanics problem, if the analytical fracture tip solution can be added to the framework of the finite element discretization, predicting fracture tip fields may be improved. This will results in increase in the number of degrees of freedom.

The partition of unity finite element method (PUFEM) using the concept of enrichment functions along with the partition of unity property, can help to obtain the following approximation of the displacement within a finite element.

$$u^h(x) = \sum_{j=1}^{m} N_j(x)(u_j + \sum_{i=1}^{n} P_i(x)a_{ji}) \quad \text{.....Eq 2.20}$$

Where, pi(x) are the enrichment functions and a_{ji} are the additional unknowns or degrees of freedom associated to the enriched solution m and n are the total number of nodes of finite elements and the number of enrichment functions p_i.

2.5.2 Enrichment Function

In two-dimensional problems, fracture modeling is characterized using of two different types of enrichment functions:

1. The Heaviside Function

For the elements completely cut by the fracture, The Heaviside function H(x) is applied for enrichment. The splitting of the element by the fracture results in a jump in the displacement field and the Heaviside function provides a simple mathematical approach to model this kind of behavior.

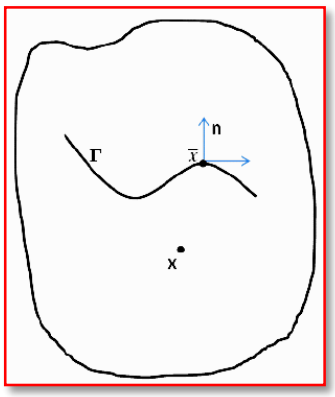

Figure 2.15: Evaluation of Heaviside function

For a continuous curve Γ, representing a fracture within the deformable body Ω, we can consider a point x(x, y) in Ω. The objective is to determine the position of this point with respect to the fracture location. If the closest point belonging to Γ is $\bar{x}(\bar{x},\bar{y})$ and the outward normal vector to Γ in $\bar{x}$ is n, the Heaviside function might be defined as follows:

$$H(x,y)=\begin{cases}1 & \text{for } (x-\bar{x}).n>0\\ -1 & \text{for } (x-\bar{x}).n<0\end{cases} \quad \text{.....Eq 2.21}$$

This function introduces the discontinuity across the fracture faces.

2. Asymptotic Near-Tip Field Functions

For those elements that are not completely fractured and containing fracture tip, the Heaviside function cannot be used to approximate the displacement field in the entire element. For the fracture tip, the enrichment functions originally introduced by Fleming for use in the element free Galerkin Method. These four functions describe the fracture tip displacement field. The first function is discontinuous at the fracture tip.

$$[F_\alpha(r,\theta),\alpha=1]=\begin{cases}\sqrt{r}\sin\left(\frac{\theta}{2}\right)\\ \sqrt{r}\cos\left(\frac{\theta}{2}\right)\\ \sqrt{r}\sin\left(\frac{\theta}{2}\right)\sin\theta\\ \sqrt{r}\cos\left(\frac{\theta}{2}\right)\sin\theta\end{cases} \quad \text{.....Eq 2.21}$$

In this formulation r,θ are polar coordinate defined at the fracture tip. The above functions can reproduce the asymptotic mode I and mode II displacement fields in LEFM, which represent the near-tip singular behavior in strains and stresses. These functions significantly improve the accuracy of calculation of K_I and K_{II}.

The term $\sqrt{r}\sin\left(\frac{\theta}{2}\right)$ is discontinuous and therefore can represent the discontinuous behavior at the fracture tip. The remaining three functions are used to enhance approximation of the solution in the neighborhood of the fracture tip.

The circled nodes are the nodes of elements completely cut by the fracture and therefore enriched with Heaviside function. The nodes with Green Square are containing fracture tip and are enriched by fracture tip special function mentioned in equation above.

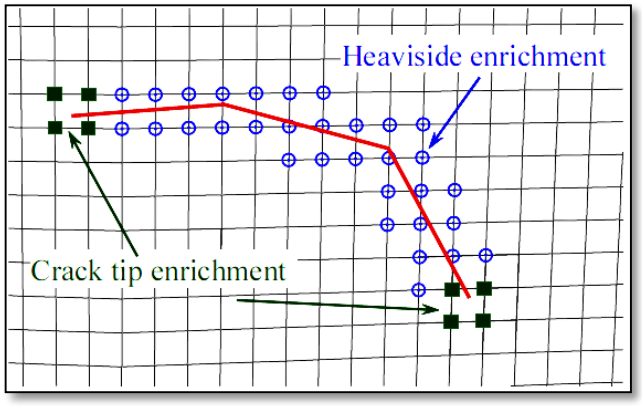

Figure 2.16: Enriched nodes in the XFEM. Circles: nodes with 2 additional DOFs. Squares: nodes with 8 additional DOFs [49].

Generally for the purpose of fracture analysis, the enrichment functions typically consist of the near tip asymptotic functions that capture the singularity around the crack tip and a discontinuous function that represents the jump in displacement across the crack surfaces. The approximation for a displacement vector function with the partition of unity enrichment [45][47][48][51].

$$u = \sum_{I=1}^{N} N_I(x)[u_I + H(x)a_I + \sum_{\alpha=1}^{4} F_\alpha(x)b_I^\alpha] \quad \text{.....Eq 2.22}$$

Where **u** is the displacement vector

$N_1(x)$ is the shape functions which applies to all nodes in the model

u_1 is the nodal displacement vectors

H(x) is the jump function and applies to nodes whose shape function support is cut by the crack interior.

a_I is the nodal enriched degrees of freedom vector.

$F_\alpha(x)$ is the asymptotic crack tip functions.

b_I^α is the nodal enriched degree of freedom vector.

The third term in the right side is applies to nodes shape function support is cut by the crack tip.

2.5.3 Level set Method for Modeling Discontinuities

In some cases numerical simulations include moving objects, such as curves and surfaces on a fixed grid. This kind of modeling and tracking is difficult and requires complex mathematical procedure. The Level set Method (LSM) is a numerical technique that can help solving these difficulties. The key point in this method is to represent moving object as a zero level set function.

To fully characterize a fracture, two different level set functions are defined:

1. A normal function, φ(x)
2. A tangential function, ψ(x)

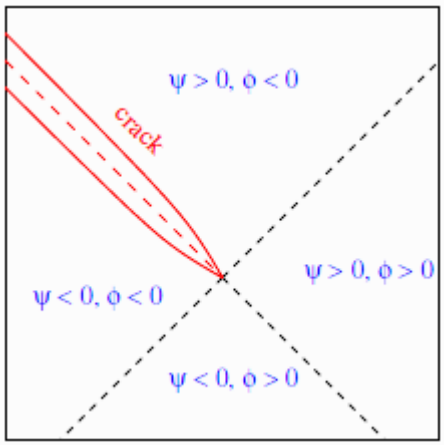

Figure 2.17: Construction of level set functions [48]

For the evaluation of the signed distance functions, assume Γ_c be the fracture surface and x the point we want to evaluate the φ(x) function. The normal level set function can be defined as

$$\varphi(x) = (x - \bar{x}).n \text{ Where } \bar{x} \text{ and n are defined previously.}$$

The tangential level set function ψ(x) is computed by finding the minimum signed distance to the normal at the fracture tip. In case of an interior fracture, two different functions can be applied. However, a unique tangential level set function can be defined as

$$\psi(x) = \max(\psi_1(x), \psi_2(x)) \quad \text{.....Eq 2.23}$$

In conclusion, referring the figure above it may be written as follows:

$$\begin{cases} \text{for } x \in \Gamma_{cr} & (x = 0) \quad \text{and} \quad \psi(x \le 0) \\ \text{for } x \in \Gamma_{tip} & (x = 0) \quad \text{and} \quad \psi(x = 0) \end{cases} \quad \text{.....Eq 2.24}$$

Where Γ_{tip} indicates the fracture tips location.

2.5.4 Implementation of XFEM in Abaqus

In ABAQUS (A powerful commercial software package, see 4.12), when the crack propagation is simulated using XFEM, the near tip asymptotic singularity (the third term in the equation above) is not needed, and only the displacement jump across a cracked element (the second term in equation above) is considered. Therefore, the crack-tip has to propagate across an entire element at a time to avoid the need to model the stress singularity [51]. Level set method in ABAQUS is a numerical technique for describing a crack and tracking the motion of the crack. It couples naturally with XFEM and makes possible the modeling of 3D arbitrary crack growth without re-meshing [50]. Phantom nodes, which are superimposed on the original real nodes, are used to represent the discontinuity of the cracked elements. The phantom node is

completely constrained to its corresponding real node when the element is intact; while the phantom node splits from the real node when the element is cut through by a crack. [51]

XFEM in ABAQUS makes crack modeling easy and accurate and allows cracks to be modeled independent of the mesh. Allows simulation of initiation and propagation of discrete crack along an arbitrary, solution-dependent path without requirement of re-meshing and it supports contour integral evaluation for stationary cracks [47].

The fracture surfaces and the fracture tip location in Abaqus are identified with a numerical procedure based on Level se Method. Once the mesh discretization has been created, each node of the finite element grid is characterized with its three coordinates with respect to the global coordinate system and two additional parameters, called PHILSM and PSILSM. These parameters are nonzero only for the enriched elements and they might be easily interpreted as the nodal coordinates of the enriched nodes in a coordinate system centered at the fracture tip and whose axes are, respectively, tangent and normal to the fracture surfaces at the fracture tip [54].

In ABAQUS, the two cracks states can be predictable [47][50][51]. These are:

1. Stationary cracks
2. Propagating cracks.

There are two distinct types of damage modeling for propagating cracks within an XFEM framework. These are:

1. Cohesive Segment Approach, and
2. Linear Elastic fracture mechanics (LEFM) Approach based on Virtual Crack Closure Technique (VCCT).

1. Cohesive Segment Approach

It can be used for brittle or ductile material fracture application. Uses traction separation laws and it follows the general framework for surface based cohesive behavior. The damage properties (Criteria) are specified as part of the bulk material definition.

The pressure over closure relationship governs the behavior when the crack is "closed" and cohesive behavior contributes to the contact normal stress when the crack is "open". [8]

Crack initiation refers to the beginning of degradation of the cohesive response at an enriched element. The process of degradation begins when the stresses or the strains satisfy specified crack initiation criteria [8] [19] [23]. Crack initiation criteria in ABAQUS are available based on the stress and strain. These are:

- Maximum principal stress (MAXPS) and Maximum principal strain (MAXPE)

$$f = \left\{ \frac{\langle \sigma_{max} \rangle}{\sigma^0_{max}} \right\} \quad \text{.....Eq 2.25}$$

$$f = \left\{ \frac{\langle \varepsilon_{max} \rangle}{\varepsilon^o_{max}} \right\} \quad \text{.....Eq 2.26}$$

- Maximum nominal stress (MAXS) and Maximum nominal strain (MAXE)

$$f = \max\left\{ \frac{\langle \sigma_n \rangle}{N_{max}}, \frac{\sigma_t}{T_{max}}, \frac{\sigma_s}{S_{max}} \right\} \langle \sigma_n \rangle = \{ \sigma_n \text{ for } \sigma_n > 0 \text{ and } 0 \text{ for } \sigma_n < 0 \quad \text{...Eq 2.27}$$

$$f = \max\left\{ \frac{\langle \varepsilon_n \rangle}{\varepsilon_n^{max}}, \frac{\varepsilon_t}{\varepsilon_t^{max}}, \frac{\varepsilon_s}{\varepsilon_s^{max}} \right\} \langle \varepsilon_n \rangle = \{ \varepsilon_n \text{ for } \varepsilon_n > 0 \text{ and } 0 \text{ for } \varepsilon_n < 0 \quad \text{.....Eq 2.28}$$

The damage initiation criterion is satisfied when $1.0 \leq f \leq 1.0+f_{tol}$ where f_{tol} is auser-specified tolerance value (default is 0.05).

- Quadratic nominal stress (QUADS) and Quadratic nominal strain (QUADE)

$$f = \left(\frac{\langle \sigma_n \rangle}{N_{max}}\right)^2 + \left(\frac{\sigma_t}{T_{max}}\right)^2 + \left(\frac{\sigma_s}{S_{max}}\right)^2 \quad \text{.....Eq 2.29}$$

$$f = \left(\frac{\langle \varepsilon_n \rangle}{\varepsilon_n^{max}}\right)^2 + \left(\frac{\varepsilon_s}{\varepsilon_t^{max}}\right)^2 + \left(\frac{\varepsilon_t}{\varepsilon_t^{max}}\right)^2 \quad \text{.....Eq 2.30}$$

The symbol $\langle\ \rangle$ is called Macaulay bracket with the usual interpretation. The Macaulay brackets are used to signify that a purely compressive stress state does not initiate damage[42][52].

2. Virtual Crack Closure Technique (VCCT)

This method is more appropriate for fracture propagation problems in brittle materials. In this method, only the displacement jump function in cracked element is considered and the fracture has to propagate the entire element at once to avoid the need to model the stress singularity. The strain energy release rate at the fracture tip calculated based on the modified virtual crack closure Technique (VCCT). Using this approach fracture propagation along an arbitrary path can be simulated without the need to fracture path being known a priori.

The modeling technique is similar to the XFEM-based cohesive segment approach. In this method also phantom nodes are introduced to represent the discontinuity of the enriched elements. The fracture criterion satisfied when the equivalent strain energy release rate exceeds the critical strain energy rate at the fracture tip in the enriched element [50].

2.6 Related Papers

Yongming Liuet. al.[6] go through an efficient 3D FEM elastic-plastic formulation to predict a subsurface crack growth of railway wheels under deterministic rolling contact fatigue loading consideration modeling which represents realistic wheel and rail profiles and gives accurate stress response under rolling contact condition without considering the thermal loading of the wheel. In their parametric study, it tries to analyze the effect of different Wheel diameter, Vertical loading, Crack length, crack orientation, Crack depth, and Crack face friction coefficients were studied on the Stress intensity factor of the subsurface crack.

Azadeh Haidari and Parisa Hosseini Tehrani [17] tried to investigate the effect of the thermal load in addition to the Mechanical load for Fatigue life of a cracked tread brake wheels. The article assumes that the wheel has an elliptical crack in definite depth of the tread surface and thermal load which is imposed on the wheel was induced on the wheel was induced from the frictional heat between the wheel and brake block. While the Mechanical loads are considered to be frictional force between wheel and rail and braking pressure. In this article, the pressure distribution along the wheel-rail contact patch while rotating was modelled using a 3D FE formulation and the translatingwheel-rail interface contact pressure was modelled by Hertz contact theory. And the final results showed that Thermo-Mechanical load coupling has a greater (non-negligible) effect than only Mechanical load consideration.

M.Wallentin et. al. [25] investigated railway wheel crack that originate from wheel flats induced by wheel/rail sliding and exposed to Rolling contact loads and residual stresses numerically using LEFM (state of shakedown) mode stress intensity factors for Mode I, II and III by applying a recent influence function method based on Betti's reciprocating theorem. The article considered Vertical component, a circumferential component and lateral component of the

total contact force and the residual stresses are due to the high temperature gradients and the following plastification and phase transformation that occur when the wheel slides on the rail.

Nagvendra Kumar Kanoje et. al. [10] studied EPFM Analysis of subsurface crack beneath a wheel by simulating dynamic conditions i.e having an assumption to represent like practical conditions such as speed, coach load and interaction to obtain contact pressure and its effect and significance on the wheel under defect. They used of Kinematic hardening and Elastic-plastic material of wheel. The wheel is moving on the rail with some angular velocity and having an elliptical crack on the wheel flat section using ABAQUS simulating software. The result evaluated parametric studies like crack orientation, vertical load, speed at 0^0, 20^0 Crack orientation, crack length, crack depth along with the J-integral.

S. Caprioli et. al.[12] investigate the impact of thermal loading imposed by block braking on the residual wheel tread cracking. A two dimensional elasto-plastic axisymmetric thermo-mechanical stress FE model of the wheel was used. And two severe load cases were considered to elucidate how the risk of crack formation behavior can be assessed and how resulting crack depths can be linked to the applied thermal loading i.e Brake malfunctioning and severe stop braking. The material model employed for the combined thermal and structural analysis incorporates linear kinematic hardening. After the formulation and Temperature determination, Fracture mechanics analysis of a semi-elliptical surface crack of the wheel was conducted. By varying the ratio of the minor and major semi-axis length of the surface crack, the authors obtain different critical crack depths for both load cases compared to the resulted stress intensity factor and the linearized fracture toughness of the wheel. The final results showed that fully functional brake systems are not likely to induce thermal crack propagation under normal stop braking.

M.Kracalik, W.Daves, T.Antretter[53] deals with finite element computations of crack driving forces for a surface crack in a rail under cyclic elastic-plastic conditions during wheel/rail contact. A straight crack normal to the surface is investigated; the examined parameters are influences of wheel load, slip, residual stresses, crack lengths and mesh around the crack tip on the crack driving forces especially the J-integral. The Chaboche material model was taken and R260 parameters were used to simulate the plastic behavior of the rail. The study assumed plane strain conditions and mechanical contact loading with flat contact surfaces. Thermal, metallurgical and chemical effects are not considered. The further analysis based on the parametric study revealed that higher mechanical loading is not directly related to a higher crack driving force. A mixed crack mode is dominant in the wheel/rail contact case.

D.Peng et. al.[55] tries to provide a method for sliding thermal fatigue crack growth in the rail freight rail wheel under stop braking load spectrum.

Sara Caprioli [56]investigated the relative severity of radial (Thermal) and inclined rolling contact fatigue surface cracks of equal depth in a railway wheel using a three dimensional FEA of a cracked wheel sector subjected to contact loading. Response is quantified by relative displacements of nodes close to crack tip and at the crack mouth. Highly inclined cracks give the highest magnitudes of crack tip shear displacements, which is the dominant deformation mode. Braking conditions are found to open the crack mouth. Initially higher temperatures on thermal cracks cause increases crack tip deformation and opening of the crack; where after subsequent mechanical load cycles impose crack closure.

Lei Wuet.al.[57] Used a FEM to study thermal-elastic-plastic deformation and residual stress after wheel sliding on a rail. The consideration of sliding contact between the wheel and the rail is restricted to a two dimensional contact problem. The repeated sliding contact process is simulated by translating the

normal contact pressure and the tangential traction across the rail surface. The normal contact pressure is idealized as the Hertzian distribution, and the tangential force is modeled by coulomb model. The results indicate that the wheel/rail friction thermal load has significant influence on the residual deformation, plastic strain and residual stress at the rail surface.

Sara Caprioli et.al. [58] present the thermal cracking of railway wheel treads using a combined experimental and numerical approach and results from controlled brake rig tests of repeated stop braking cycles for a railway wheel in rolling contact with a so called rail wheel. Test conditions are then numerically analyzed using FE simulations that account for the thermo-mechanical loading of the wheel tread. For the studied stop braking case, thermal cracks are found in the wheel tread after few brake cycles. Results from thermal imaging reveal a frictionally excited thermos-elastic instability phenomenon called "banding" where the contact between brake block and wheel occurs only over a fraction of the block width. This condition results in locally high temperatures. The numerical analysis assess ratcheting response of the wheel tread material under operational conditions corresponding to two types of banding patterns and also a case of uniform heating. Fatigue life predictions are estimated from the evaluated ratcheting response using a simplified accumulated rule.

2.7 Summary

Many researchers go through cracking and failure of a railway wheels under different loading conditions. Among other researcher some of them focus only on the crack growth due to mechanical loads without the consideration of thermal stresses induced during braking, slippage of the wheel or due to the skating of the wheel due to jamming of brakes. The rest considered the thermally induced cracks of wheels and their propagation scheme. Few of researchers considered both of the loading conditions with a mechanical load and thermal load of a very slow sliding velocities i.e a low frictional heating level with questionable FE analysis method.

This thesis work has got the value of filling the gap of considering cracks induced from larger sliding velocity due to the brake jamming and static mechanical load by utilizing an efficient mathematical formulation found in ABAQUS known as extended finite element method (XFEM).

Chapter Three

Analysis and Modeling

3.1 Boundary and Loading Computation

3.1.1 Mechanical Load

During the Mechanical and Thermal load computations, the basic boundary conditions are taken from the data of Addis Ababa Light Rail Transit system of the Ethiopian Railway Corporation as a case study. The Material properties that can never be found in the LRT project were taken from different published papers which are cited along with them.

Table 3.1: Data of the Boundary conditions[59]

Vehicle Parameters	Amount
Train Maximum capacity = 317 Passengers Train weight=W_T=44,000kg	m_T=64,000kg
Number of Axles per vehicle	6
Number of wheels per vehicle	12
Max. Velocity of the wheel during wheel lockup, V_s	80 km/hr =22.2 m/s
Emergency brake deceleration, D_{eb}	-1.5m/s^2
Average acceleration, a	1m/s^2
Vehicle wheel diameter, d_w	660 mm for new wheel
Friction coefficient of the Dry condition	0.4

The Normal load imposed on a single wheel: N_w

$$N_w = \frac{\text{The Total vehicle load},\ N_T}{\text{Number of wheels per Train},\ n} = \frac{627{,}840\ \text{N}}{12} = 52{,}320\ \text{N}$$

Contact Patch Geometry

During the contact analyses, a linear elastic material model was used for both the wheel and rail by taking advantage of Hertz contact theory since the contact patch approximation is good enough with that of the Kalker's CONTACT/FASTSIM software. This theory describes this fact that when two solid materials are compressed to each other by the Normal load imposed on them, their contact area is formed. Shape and the value of the contact area between two elastic materials are at static mode. The material property of the wheel and the rail is listed in Table 4.2 below. In the case of the wheel, R7T is selected as most of passenger wheels are made currently using it and for the rail [64].

Table 3.2: Material properties applied for contact geometry analysis

Modulus of Elasticity			
	Wheel	E_1	206 GPa
	Rail	E_2	210 GPa
Poisson Ratio			
	Wheel	v_1	0.27
	Rail	v_2	0.3

The studied wheel in contact with the rail is S1002 profile and the rail is the European standard rail type UIC60. The Rolling Radius of the wheel R_1 is 660 mm, the lateral rolling circle radius of the wheel is 70 mm. And the rolling curve radius of the rail is r_2=300 mm and R_2=∞ (See Appendix D).

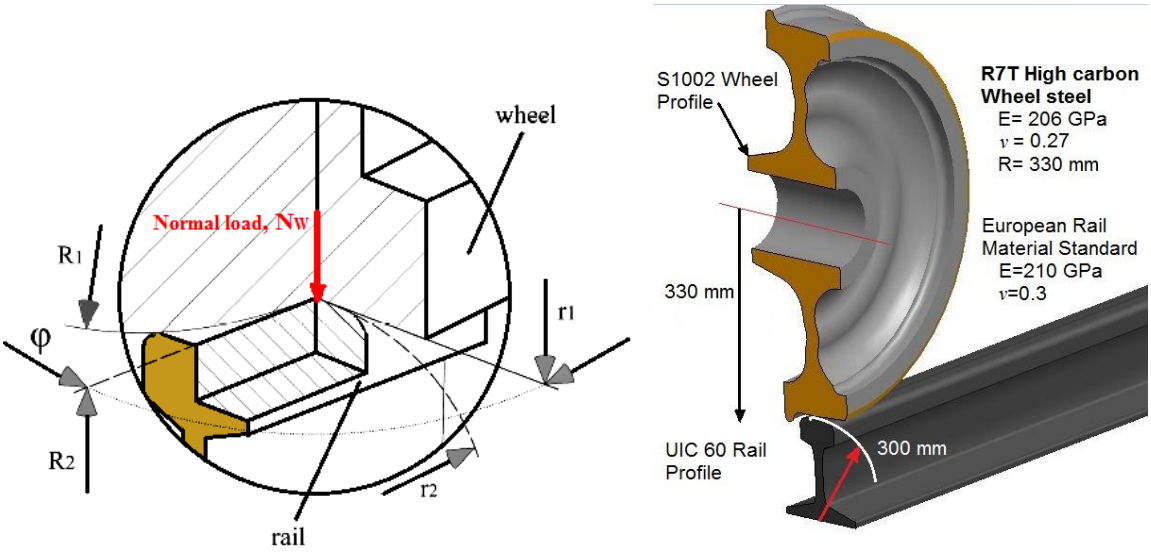

Figure 3.1: Wheel-Rail contact Parameters **a**). [57] **b)**. wheel parametrs taken

The Equivalent Radius Values:

$$k_{11}=\frac{1}{R_1}=3.03\times10^{-3}mm^{-1}$$

According to [64], the Equivalent radius k_{12}can be determined from

$$X=\frac{3.358537058}{100}Z+\frac{1.565681624}{1000}Z^2-\frac{2.810427944}{100000}Z^3+\frac{5.844240864}{10^8}Z^4-\frac{1.562379023}{10^8}Z^5+\frac{5.309217349}{10^{15}}Z^6-\frac{5.957839843}{10^{12}}Z^7+\frac{2.646656573}{10^{13}}Z^8$$

Thus, wheel curve in the point contact with rail is calculated as the following:

$$k_{12}=\frac{|Z''|}{(1+Z'^2)^{3/2}}$$

And therefore, the wheel curve radius considering 70 mm from the wheel rim is achived at X=0 is

$$r_1=\frac{1}{k_{12}}=\frac{(1+Z'^2)^{3/2}}{|Z''|}\approx-320\text{mm},$$

$$k_{12}=-\frac{1}{r_1}=-3.125\times10^{-3}\,\text{mm}^{-1}$$

k_{21}=0 since r_1 and R_2 are ∞.

$$k_{22}=\frac{1}{r_2}=3.333\times10^{-3}\ mm^{-1}$$

$$\Sigma k = 3.2386\times10^{-3}\ mm^{-1}$$

The Equivalent Radius Ratio, Ψ is

$$\Psi=\frac{1}{\sum k}\sqrt{(k_{11}-k_{12})^2+(k_{21}-k_{22})^2+2.(k_{11}-k_{12}).(k_{21}-k_{22}).\cos 2} = 0.3413$$

Therefore, for the value of Ψ= 0.3413, we have the following from **Appendix 1**.

Table 3.3: Summarized results obtained analytically

Parameters	Value	Parameters	Value
k_{11}	3.303×10^{-3} mm^{-1}	n_a	1.2848
k_{12}	-3.125×10^{-3} mm^{-1}	n_b	0.78692
k_{21}	0	n_δ	0.9744
k_{22}	3.333×10^{-3} mm^{-1}	n_p	0.9746
$\sum k$	3.2386×10^{-3} mm^{-1}	Ψ	0.3413

The contact Patch Dimensions are therefore,

$$a = n_a\sqrt[3]{1.5N_W\frac{\eta}{\sum k}} = 7.7mm$$

$$b = n_b\sqrt[3]{1.5N_W\frac{\eta}{\sum k}} = 4.71mm$$

As per [57] finding of contact geometry using FEM and Analytical methods there is a slight deviation of **1.2 % and 6 %** for the values of a and b respectively. Using these values, I correct the values to a= 7.8 mm and b= 5 mm.

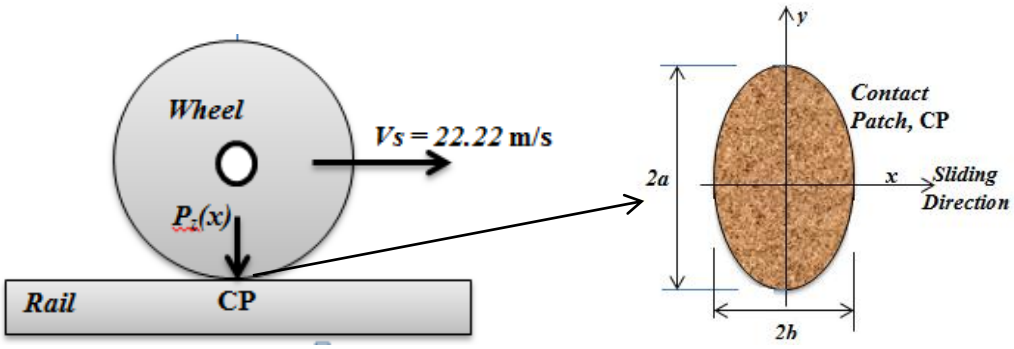

Figure 3.2: Contact patch Geometry

Where:

a = half length of the contact in Lateral Direction

b= half length of the contact in Longitudinal Direction

The Maximum contact Pressure, P_o

$$P_o = \frac{3N_W}{2\pi ab} = \frac{3(52{,}320\,N)}{2\pi(7.8\times 5)} = 650\,MPa$$

The Normal pressure distribution on the contact patch is:

$$P_z(x,y) = P_o\sqrt{1-\frac{x^2}{b^2}-\frac{y^2}{a^2}} = 650MPa\sqrt{1-\frac{x^2}{5^2}-\frac{y^2}{7.8^2}}$$

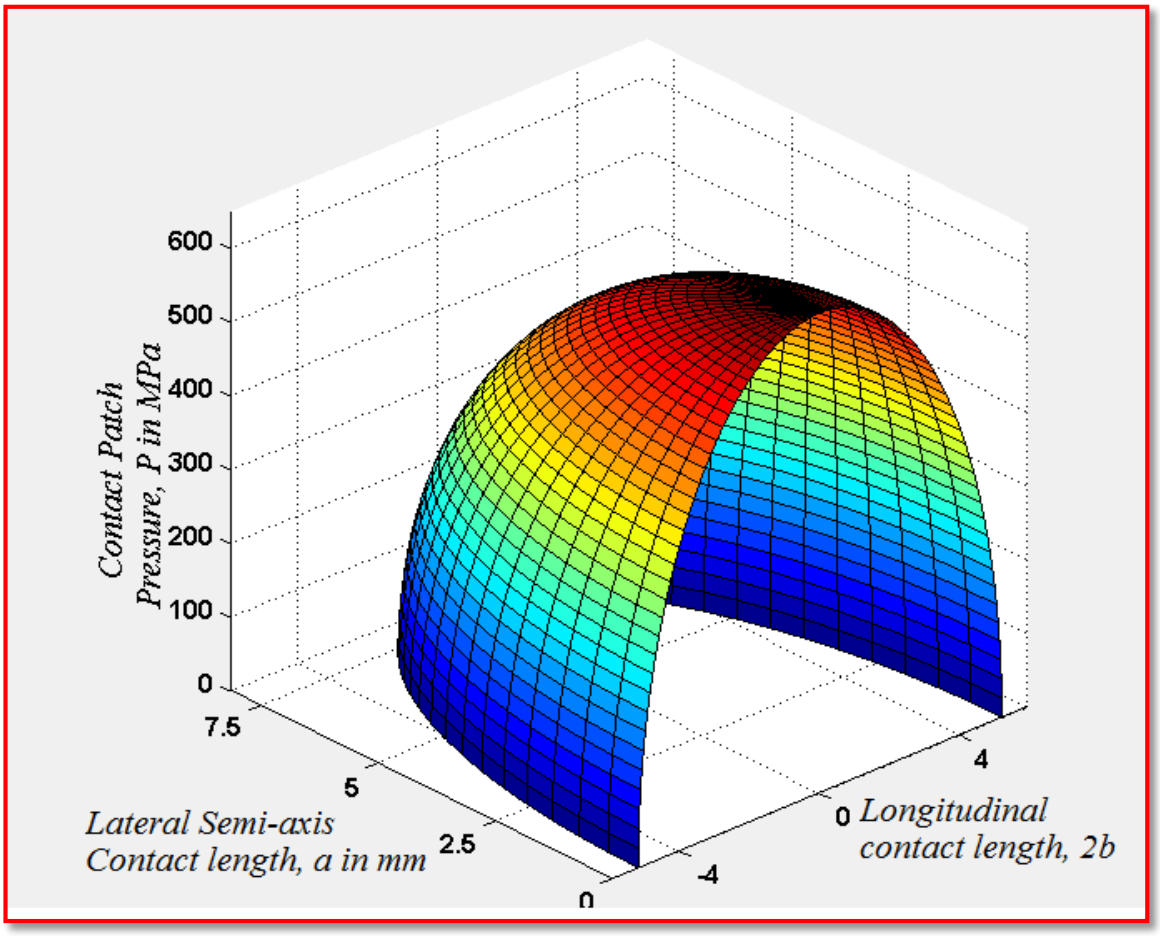

Figure 3.3: Surface Pressure Distribution on the wheel/rail CP (Sectioned)

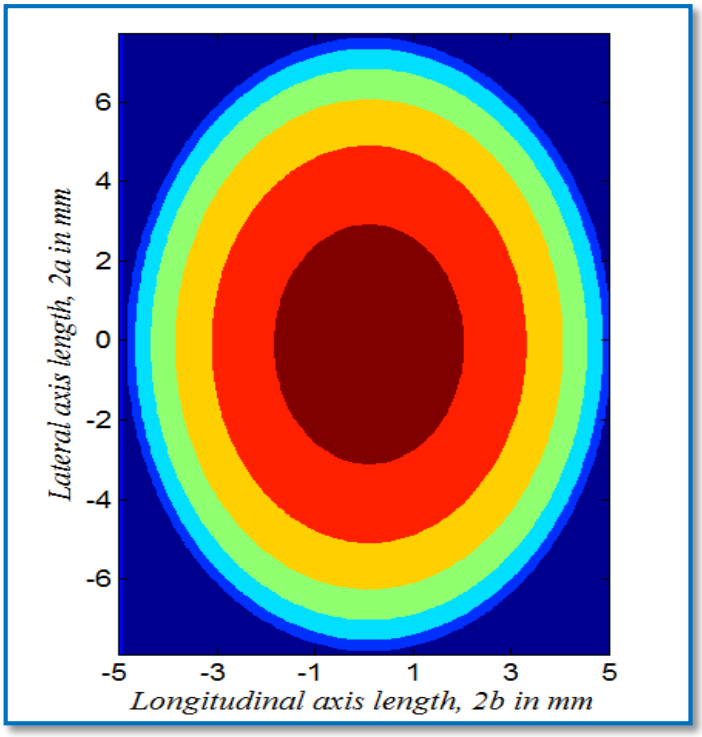

Figure 3.4: Pressure distribution contour plot

To assess the stress and Temperature fields, we have to find the Pressure distribution along the x (longitudinal) and y (Lateral) direction of the contact ellipse:

$P_z(x) = P_o\sqrt{1-\frac{x^2}{b^2}} = 650\sqrt{1-\frac{x^2}{25}}\,MPa$ is the longitudinal Pressure Distribution.

To make it simple for further analysis and the author try to substitute the elliptical contact with a linear pressure distribution graph and again to a Normal equally distributed pressure (Rectangular distribution).

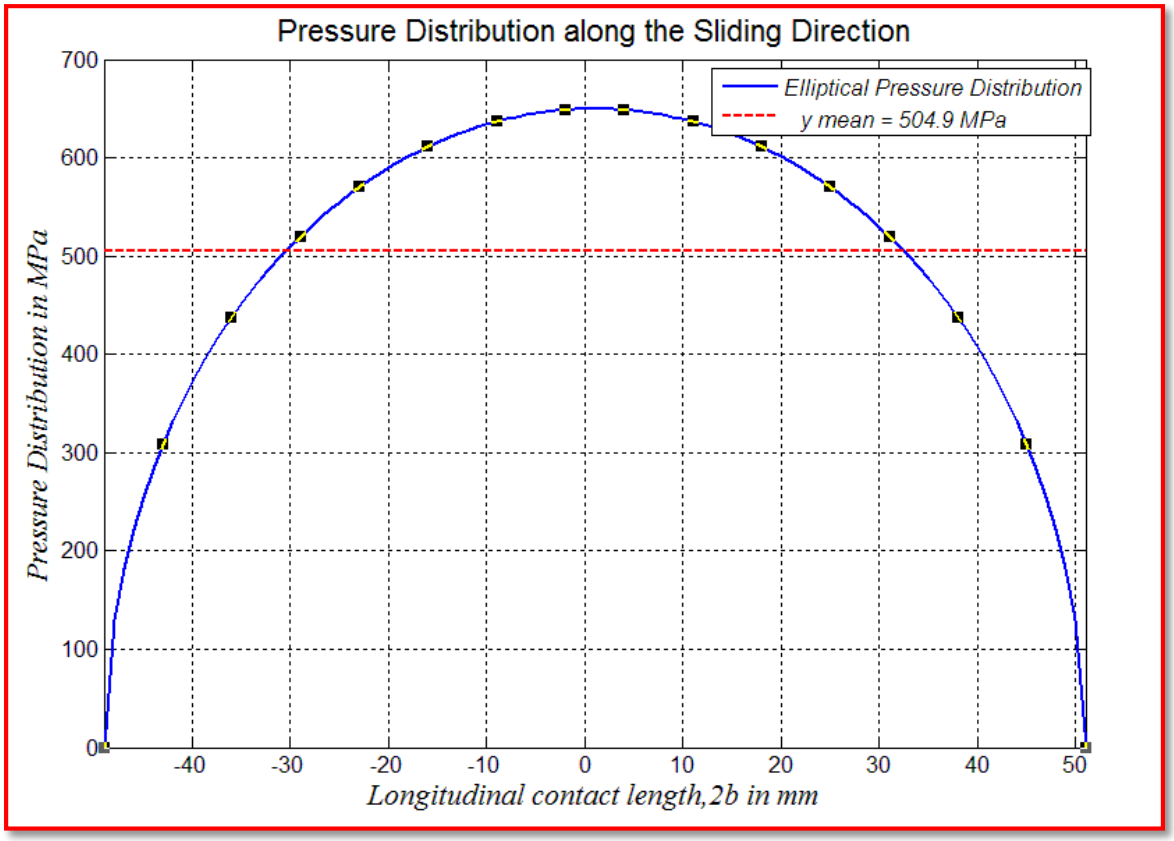

Figure 3.5: Longitudinal Contact Pressure Distribution

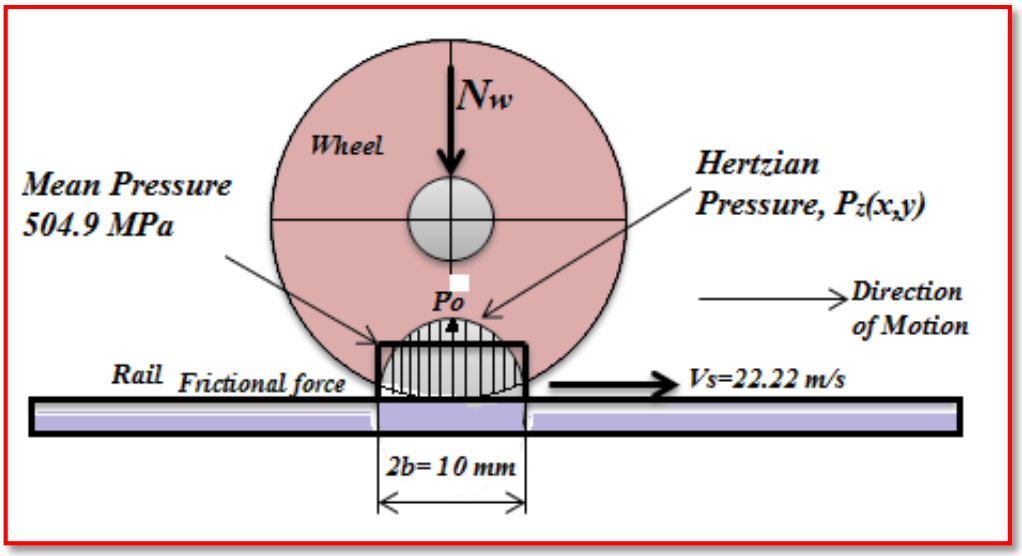

Figure 3.6: Loading condition of the wheel and rail

$P_z(y) = 650\sqrt{1 - \frac{y^2}{60.84}}$ MPa is the Lateral Pressure Distribution

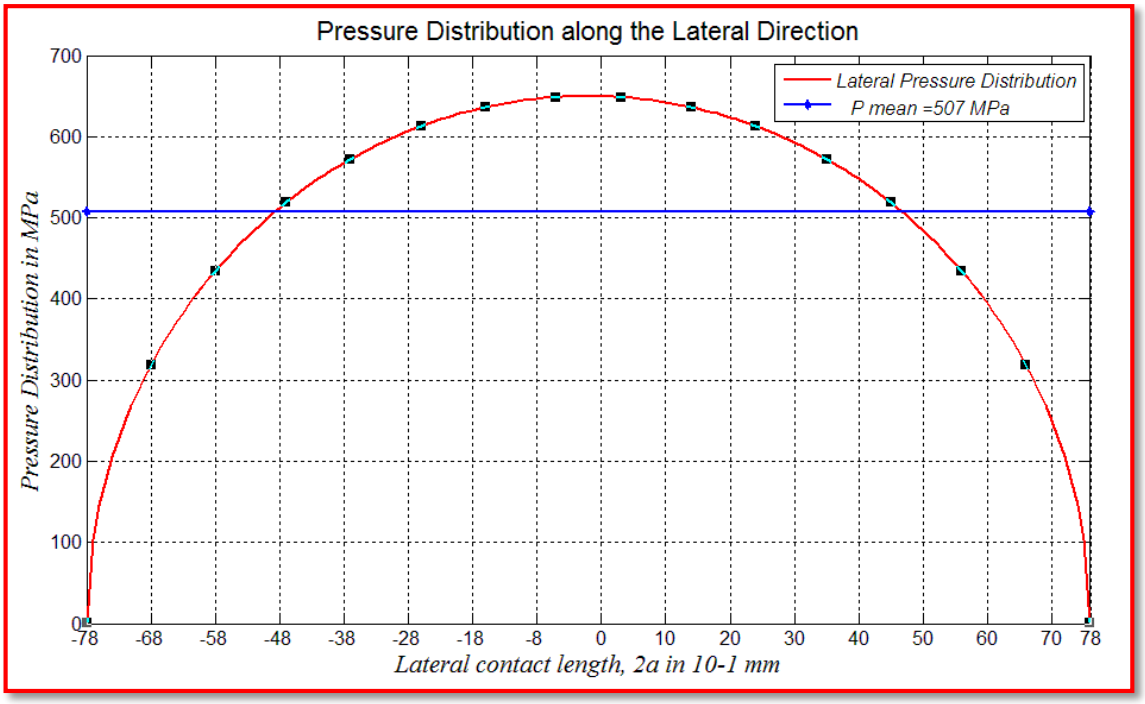

Figure 3.7: Lateral Contact Pressure Distribution

Simplification of the Contact Patch Area

Based on [20], during the application of the thermal load on the contact patch during the crack propagation analysis, the elliptical contact patch area was considered to be rectangular for simplified FE discretization and load application in the software. The half-length of longitudinal contact ellipse was about 5 mm while the half-length of the contact patch along the Lateral direction was 7.8 mm. For simplification the ellipse was substituted by a rectangle of 9 mm×13.6 mm rectangular shape which is having 122.4 mm^2 area by assuming that the resultant and the computed average thermal load imposed on the Rectangular area is the same with that of the elliptical contact patch area ($\pi \times 5 \times 7.8 = 122.52\ mm^2$).

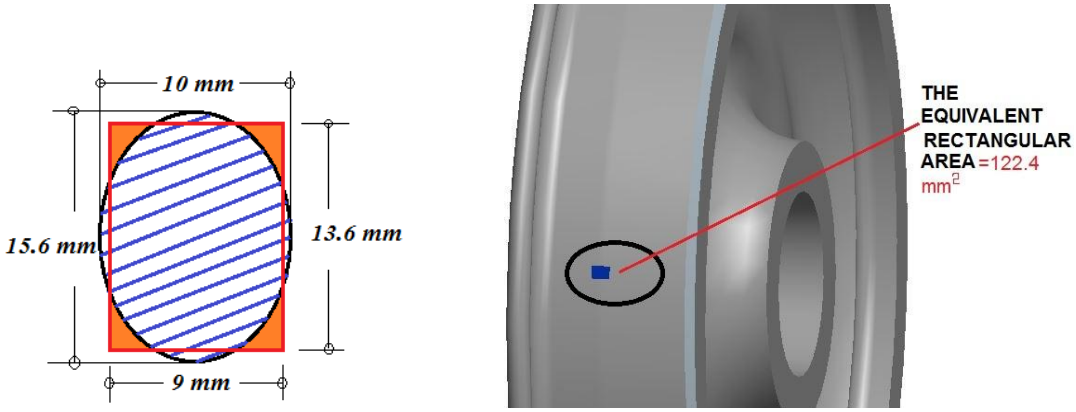

Figure 3.8: The original and the modified contact patch and their dimension

3.1.2 Frictional Heat Load

The thermal properties for the frictional heat load calculation are tabulated below:

Table 3.4: Material properties of the wheel [14] [20][35]

Parameters	Symbol	Value
Sliding velocity	V_s	22.22 m/s
Density of the material	P	7,850 kg/m^3
Specific heat capacity	c_p	540 J/kg^{o}C
Thermal Conductivity	Λ	54 W/m^{o}C
Coefficient of Thermal Expansion	A	2×10^{-5} (1/K)

During the very short time period that every point on the surface is in contact, the thermal penetration depth, δ is

Where L is the Péclet Number

$$L=\frac{bV_S}{2k} = 3924.6 \text{ and k (Thermal diffusivity)} = \frac{\lambda}{\rho c} = 12.74\times10^{-6} \text{ m}^2/\text{sec}$$

According to [20] thermal studies can be classified in to two groups according to the Peclet Number (L) i.e A small Peclet number represents a so called "Slow sliding" contact, whereas a large Peclet number represents a "fast sliding" contact. The larger the value of the Peclet Number, the less heat Penetrates below the surface, rather than resulting in only surface temperature rise. If L<0.8, there is "slow sliding" contact, and if L>5, the contact is "fast sliding" contact.

And the heat conduction along the longitudinal and lateral direction can be neglected and it is only along the z-direction [30].

Therefore,

$$\delta = \frac{b}{\sqrt{L}} = \frac{4.5\times10^{-3}\,m}{\sqrt{3924.6}} = 7.1831\times10^{-5}\,m = 71\ \mu m$$

Where

The Total heat generated at the surface interface (*line contact*) is

$$\dot{q}_{friction}(\xi) = \mu V_s P_z(\xi) = \mu V_s P_o \sqrt{1-\xi^2} = \mu . V_s P_{Longitudinal\ mean}$$

$$\dot{q}_{friction}(\xi) = \mu V_s P_z(\xi) = \mu V_s P_o \sqrt{1-\xi^2} = \mu . V_s P_{Lateral\ mean}$$

The heat partitioning parameter based on the duration of sliding time is given in [37] and according to Eq 2.19. in our case it looks like:

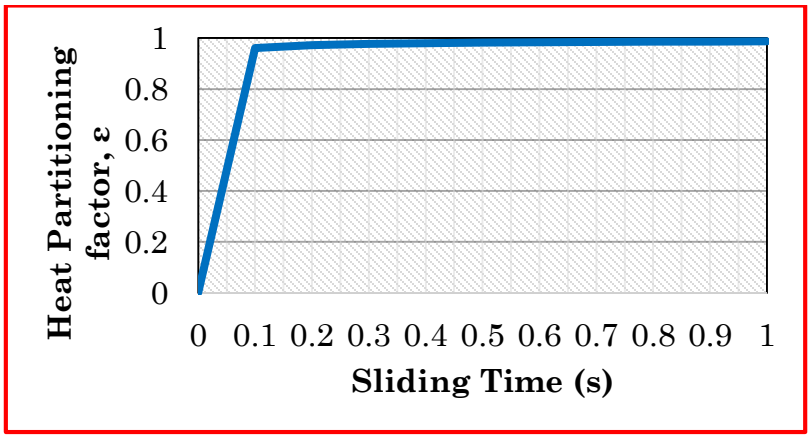

Figure 3.9: Heat Partitioning parameter Vs sliding duration at v=22.22 m/s.

The interface temperature rise between the wheel and rail considering the maximum case scenario ε=1 is can be determined from [35].

$$T_{max} = \frac{1.276\varepsilon\mu V_S P_o}{\beta_W}\sqrt{\frac{b}{V_S}}$$

By Applying Lagrange second order interpolating polynomial equation to interpolate the temperature for velocity of 22.22 m/sec gives [37] for the same loading conditions:

$$T_2(V) = \frac{(V - V_1)(V - V_2)}{(V_o - V_1)(V_o - V_2)}T(V_o) + \frac{(V - V_o)(V - V_2)}{(V_1 - V_o)(V_1 - V_2)}T(V_1) + \frac{(V - V_o)(V - V_1)}{(V_2 - V_o)(V_2 - V_1)}T(V_2)$$

Table 3.5: Interface temperature Interpolation

Sliding Velocity, V_s	Temperature, ^0C
12.91	790
22.22	$T_2(V)$ =955
25.82	1019
41.31	1297

Heat generated in different conditions:

$$\dot{q}_{friction} = \mu V_s . P_{mean\ (Longitudinal)} = 4.487\times10^9\ W/m^2 \text{and}$$

$$\dot{q}_{friction} = \mu V_s . P_{mean\ (Lateral)} = 4.506\times10^9\ W/m^2$$

The approximate and average heat on the rectangular area of contact will be

$$\dot{q}_{friction} = \mu V_s.((P_{mean\ (Longitudinal)} + P_{mean\ (Lateral)})/2)$$
$$= 0.4\times22.22\times506MPa = 4.5\times10^9\ W/m^2$$

Table 3.6: Thermo-Mechanical coupling loads and duration times

Sliding Cycle	Duration Time (sec)	Mechanical Load (MPa)	Thermal Load (MW/m^2)
Accelerating	22.22	506	2250
Constant velocity	19.7	506	4500
Brake deceleration	14.8	506	2250

The total and average Load spectrums that contribute to the crack opening stress are:

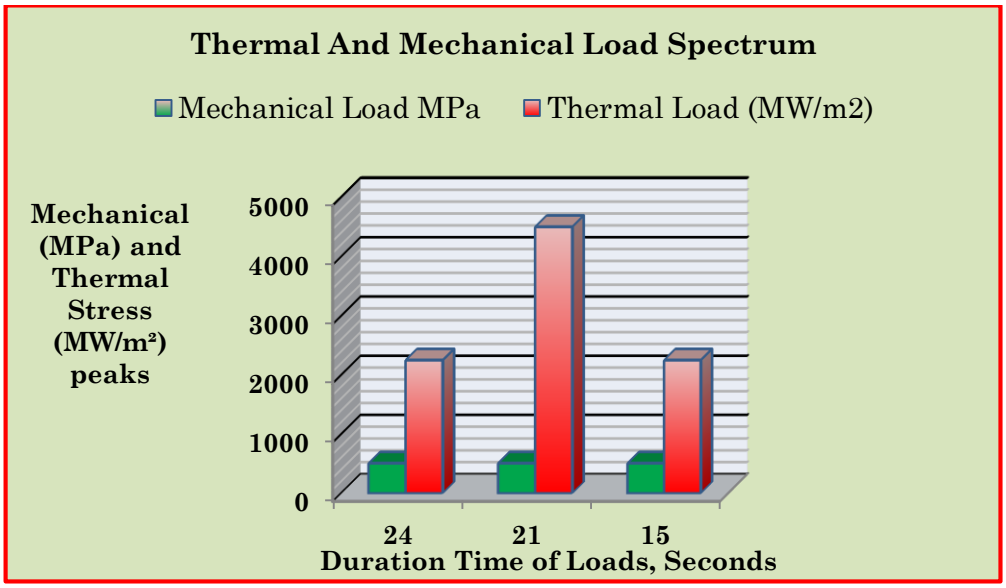

Figure 3.10: Loading spectrum during sliding of the wheel

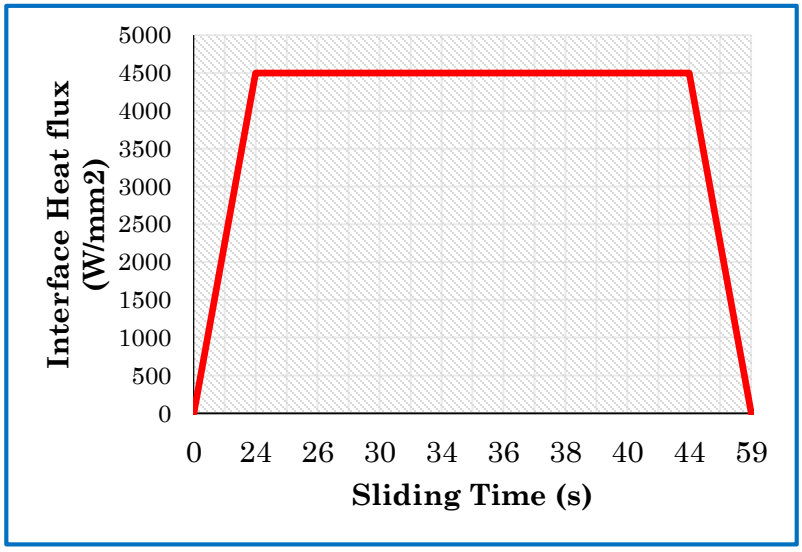

Figure 3.11: Interface Heat flux versus Sliding Time: LRT case study between two stations

For the coupled wheel thermal-stress analysis of the wheel, Boundary conditions used are: T_{surf}= 955 ^{0}C and Interface contact pressure of 506 (N/mm^2) are used. The Ambient temperature is applied at the upper end of the simplified wheel geometry.

3.2 XFEM Analysis in Abaqus

3.2.1 ABAQUS Software Package

ABAQUS is a suite of powerful engineering simulation programs based on the FEM, sold by Dassault Systems as part of their SIMULIA Product Life Cycle Management (PLM) software tools. It is written and maintained by Hibbit, Karlsson and Sorensen, Inc (HKS). It is a highly sophisticated, general purpose finite element program, designed primarily to model the behavior of solids and structures under externally applied loading [60].

The unique features of ABAQUS include:

- ABAQUS contains an extensive library of elements that can model virtually any Geometry.
- It allows importing geometry from a many different CAD software packages.
- Using ABAQUS, we can be able to use various different material models to simulate the behavior of most typical engineering.
- Designed as a general-purpose simulation tool, ABAQUS can be used to study more than just structural (stress/displacement) problems. It can simulate problems in many diverse areas.
- ABAQUS offers a wide range of capabilities for simulation of linear and nonlinear applications. Problems with multiple components are modeled by associating the geometry defining each component with the appropriate material models and specifying component interactions.
- It let to perform static as well as dynamic analysis.

ABAQUS-standard and ABAQUS-Explicit are two main analysis modules in ABAQUS. ABAQUS-standard is a full purpose analysis module that can solve a variety of problems covering linear and nonlinear problems maintaining the

accuracy and the reliability of the results. ABAQUS-Explicit is a special purpose analysis module that uses dynamic finite element formulation, which is applied to deal with the problems of transient and dynamic in nature[54].

ABAQUS-CAE is the total ABAQUS working interface that includes all the options to generate ABAQUS models, to submit and monitor jobs for analysis and also a means to review the results.

In this thesis work, ABAQUS-CAE is used for the preprocessor of different stages of the model creation starting from the creation of Part, Property and assembly, defining the step, Interaction, Load, Mesh and generating the Job from the respective module and postprocessor to extract the results using visualization module. And the post processing is done using ABAQUS/Standard.

Wheel Geometry Simplification

Since the wheel is Jammed/Locked, there is no relative motion of a wheel region near the bottom contact of the wheel and rail. For a more simplified analysis, it is better to take a small portion of the wheel to apply the loads i.e both the Mechanical and thermal loads with respect to edge crack on the surface at varying predetermined angle and depth.

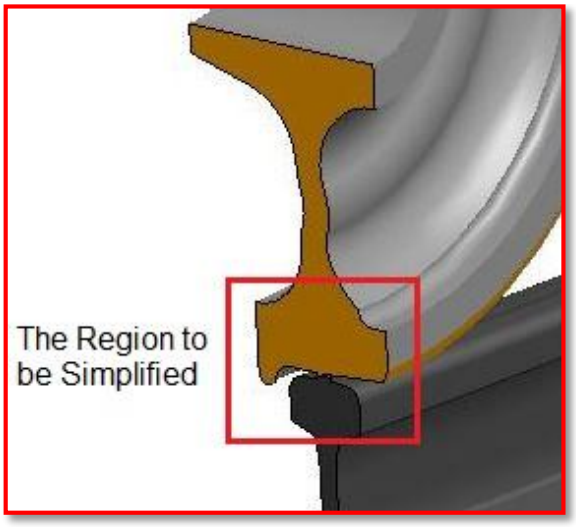

Figure 3.12: The wheel Region to be simplified

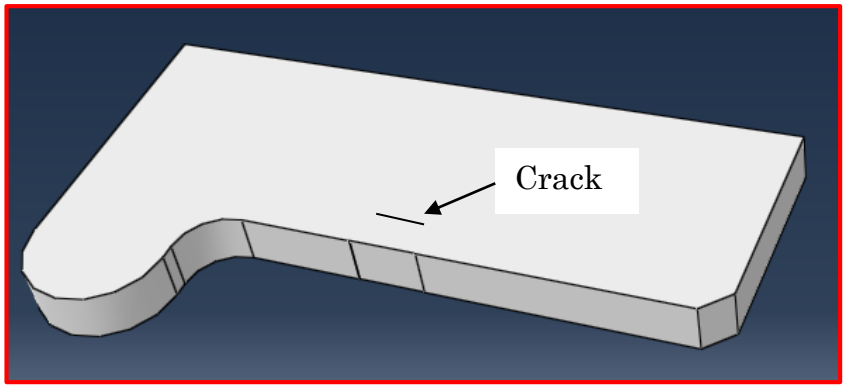

Figure 3.13: Simplified wheel geometry and crack location

3.2.2 Elastic-Plastic Wheel Material Property

Plastic deformation is defined as permanent change in shape or size of a solid body without fracture resulting from the application of sustained stress beyond the elastic limit.

Plasticity in metals is usually a consequence of dislocation within the structure. Plasticity will occur beyond the yield point of the material. Once the load exceeds the yield strength threshold, there is more of a rapid increase in stress than the elastic range, and when the load is removed some amount of the extension still exist which results in permanent deformation. [64]

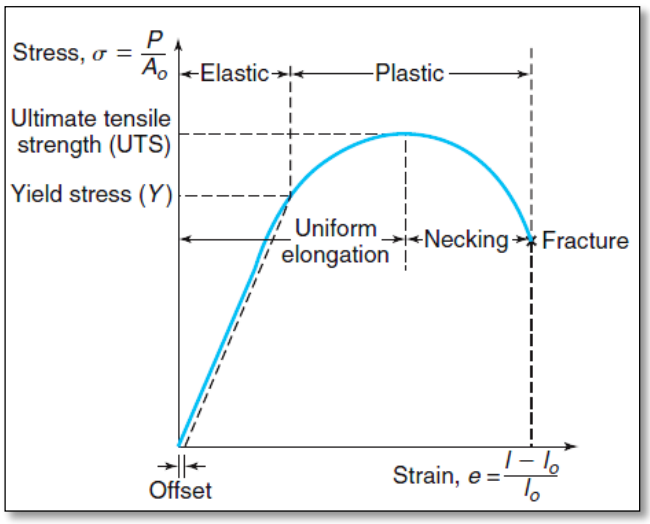

Figure 3.14: A typical stress-strain curve [65]

ABAQUS requires that the material be sufficiently defined to provide suitable for those elements with which the material is associated and for all of the analysis procedures through which the model will be run [ABQUS user manual vol.3 Materials]. To perform the elastic-plastic analysis, the elastic mechanical properties are required (which are governed by Hook's Law) because this will provide the stress-strain relationship up to the yield point but additional information is required to ensure the plastic range is accurately developed. To develop the plastic range in FEA, the Yield and plastic strain need to be manually loaded in to the material properties. If the plasticity data has not been entered into FEA ABAQUS, the stress/strain relationship will continue to be linear. This will not provide an accurate result of stress in the plastic range.

A power law work hardening model is accepted by most engineering materials such as metals and alloys approximately which is a material constitutive relation, the modified uniaxial stress-strain (σ-ε) curve of a stress free material can be expressed as [61]:

$$\sigma = E\varepsilon \text{ for } \varepsilon < \sigma_y/E$$
$$\sigma = K\varepsilon^n \text{ for } \varepsilon > \sigma_y/E \quad \text{.....Eq 3.1}$$

Where E is Elastic modulus, $\sigma_y$is yield stress; n is the work hardening exponent and $K = \sigma_y(\frac{E}{\sigma_y})^n$ is work hardening rate. When n is zero the above equation reduces to an elastic-perfectly plastic material. To completely characterize the elastic-plastic properties of a power-law material, four independent parameters, i.e, elastic modulus, E, Yield stress, σ_y,work hardening exponent, n and Poisson's ratio, υ are needed.

To define the plastic properties of a material in ABAQUS the power law hardening material model is used, a true stress strain data spreadsheet at first is generated in Excel from the Equation (Eq 4.1). Then using the equation below (Eq 4.2), plastic strain (ε_P) is calculated.

$$\varepsilon_P = \varepsilon - \frac{\sigma_y}{E} \quad \text{.....Eq 3.2}$$

System of Units in ABAQUS

Since ABAQUS doesn't specify a unit system, the user could use a unit system arbitrarily, as long as they are in consistency in one problem [61].

In this thesis, the author uses consistent basic units as:

- Newton (N) as the unit of force (load).
- Millimeter (mm) as the unit for displacement.
- Degree Celsius (^{0}C) for the unit of Temperature.
- Kilogram (Kg) for the unit of mass

Therefore, as per the unit definition the material properties used in ABAQUS are

Table 3.7: Elastic material behavior of the wheel material

Classification	Property	Value
General	Density	7850×10^{-9} kg/mm^3
Elastic Region Behavior	Modulus of Elasticity	206,000 N/mm^2
	Poisson's Ratio	0.27

The Approximate and summarized Material Properties of the wheel used in crack modeling and stress analysis are listed below:

Table 3.8: Reference mechanical property data of the material

Fracture Toughness, K_{Ic}	Yield Stress, σ_y	Ultimate Strength, σ_{us}
50MPa $\sqrt{m}$	350	500

The plastic region behavior can be represented as:

$$\text{Property} \rightarrow \text{Mechanical} \rightarrow \text{Plasticity} \rightarrow \text{Plastic} \rightarrow \text{Yield stress / Plastic strain}$$

And by using Power law, we used four data points of the yield stress/plastic strain,

Table 3.9: Plastic region behavior of the wheel material

No	Yield stress, N/mm^2	Plastic Strain, mm
1	350	0
2	370	0.00054302
3	420	0.00252333
4	500	0.00839219

The Temperature dependent thermal properties are used for the wheel material to best represent their working condition under high thermal loads during the Analysis. By assuming the increment scheme with respect to temperature, we interpolate the data available in [62]

Table 3.10: Temperature dependent thermal properties used in ABAQUS

Temperature, ^{0}C	Thermal Conductivity, $\times 10^{-3}$ W/mm^{0}C	Specific Heat, (J/Kg^{0}C)	Coefficient of Thermal expansion, 10^{-6} /^{0}C
20	54	450	20
100	58.04	487	20.5
200	63.2	520	21
300	68.34	537	21.9
400	74.5	548	22.63
500	78.6	555	22.8
600	82.7	562	22.9
800	93.9	587	23.4
1000	104.7	611	23.65

The XFEM analysis requires material information in the enriched area of crack. The maximum principal ('Maxps Damage' in ABAQUS) was selected for the damage initiation criteria. The ultimate stress/strength was used as the limiting maximum principal stress. Damage evolution was based on an energy criteria which is equivalent to the strain energy release rate ('Fracture energy' on ABAQUS), G_I and a linear softening, maximum degradation a Mode independent.

Fracture energy was estimated using the relationship below [10]

$$G_{IC} = \frac{K_{IC}^2}{E} \quad \text{.....Eq 3.3}$$

$$= \frac{\left(50 \times 10^3\right)^2}{206{,}000} = 12.136 \text{N/mm}$$

Where

G_{Ic} is the fracture energy,

K_{Ic} is fracture Toughness of the wheel material =50 MPa $\sqrt{m}$ and

E is young's Modulus of Elasticity

Crack growth problems require progressive damage, which includes softening and loss of stiffness which can cause severe convergence difficulties. Viscous regularization can be added to analysis ensuring that tangent stiffness matrix is positive definite thereby improving convergence rates. It should be noted that too much stabilization can cause negatively influence of the solution and produce even non-physical results. The value is within the acceptable limit so the Damage stabilization cohesive coefficient is taken as 1E-06 [42].

Convergence Issue handling

The default time incrementation parameters in ABAQUS are set to achieve some good performance for smooth behavior. However, for discontinuous analysis such as crack growth, the default time integration scheme may result in premature cutbacks and termination. Abaqus/standard abandons iterations and cutbacks the time increment if it finds the residuals are increasing in two consecutive iterations after I_o equilibrium iterations. Another routine check performed is that for logarithmic rate of convergence, based on which the total number of iterations are estimated; if this estimation exceeds I_c,

Abaqus/standard reduces the time increment. This check is performed after I_R iterations. The default values of I_o and I_R is 4 and 8 respectively for the continuous domain. For discontinuous domain analysis the values of I_o and I_R are modified as 8 and 10, respectively, cutbacks and reduction in time incrementation are delayed due to it. Also, the number of attempts for each increment was also increased for their convergence rates.

Therefore, to handle the difficulty of the XFEM convergence issues the minimum the minimum time step was set to 1E-10and the number of increments was increased to 100,000 to prevent premature abortion of the step input.The initial time step for smooth curve simulation a value of 0.01 was used. And beside this the following changes were also made in the step module:

- Step Module → General solution controls → Manager → Edit step → Specify→ Time increment→ Discontinuous Analysis→ more I_A=20→ok.
- Step Module→ Other →General Solution controls→ Manager →Edit Step→ Time Increment → Select Discontinuous Analysis.
- Step Module → Step→ Step Manager→ Edit →Automatic Stabilization→ Specify Dissipation Energy fraction→ Accept defaults.

Mesh Details

The mesh process consists of partitioned three wheel sections and applied different element types and edge seeds for each. The middle section (Part 1) consist of 20×40×10 seeds with an Element type of C3D8 (An 8-node linear brick, full integration) and Part 2 and 3 with an edge seeds in Figure below and an Element type of C3D8R (An 8-node linear brick, reduced integration, hourglass control). This will help reduce computational cost since full integration elements are only required where cracking takes place. The part is meshed with a total of 21,370 elements.

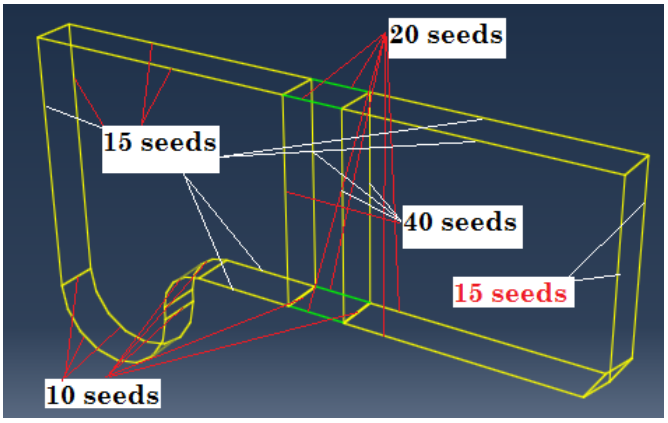

Figure 3.15: Edge Seed sizes assigned for the part of the wheel.

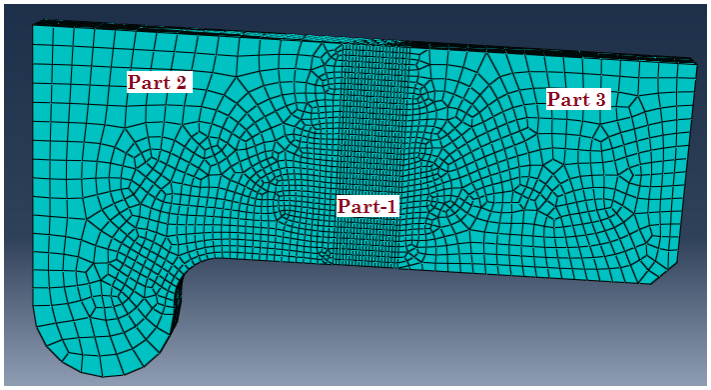

Figure 3.16: Mesh Details

3.2.3 Parametric study

To see the sensitivity of the crack propagation behavior, different crack size and inclinations were used. These are:

To represent the subsurface cracks, a horizontal planar shell was used at a depth of 5 mm from the contact surface point. To study the effect of initial crack length we used 5 mm, 8 mm and 10 mm cracks. For the subsurface crack case, angle of inclination used are 30^0, 60^0, and 90^0.

Chapter Four

XFEM Result and Discussion

The Analysis performed in Abaqus XFEM was performed in two different load considerations with varying parameters for sensitivity studies. The first analysis was done using a static mechanical load only which is 506 MPa and the second is by considering the combined temperature rise from 20^0C to 955^0C by specifying in the predefined field at the surface and mechanical load to see the effect of the frictional heat load to assess the seriousness of the problem of skidding due to Jamming of brakes.

To evaluate the crack tip maximum principal stress and Equivalent plastic strain we simulate the wheel with the crack extension value Δa=0.25 mm [56] and at varying crack inclination angle at a depth of 5mm. Even though STATUS XFEM output in the XFEM analysis is red for the stable crack surrounding the crack surface and different color spectrums for a growing cracks and PHILSM and PSILSM are the two level set values to represent the crack from the normal and tangent directions this parameters are not sufficient parameters to understand the crack behavior with increasing length. The Equivalent plastic strain (PEEQ) is used here to evaluate the yield condition of the wheel bonds. In an isotropic hardening plasticity theory, for most materials the PEEQ is defined as $\sqrt{\frac{2}{3}\mathrm{d}\varepsilon^{\mathrm{pl}} : \mathrm{d}\varepsilon^{\mathrm{pl}}}$, and is the total accumulation of plastic strain to define the yield surface size [64].

The damage initiation criteria is based on the 'Maximum principal stress' criterion which is expected to be 500 MPa to initiate the crack propagation stage.

4.1 XFEM Abaqus Results

4.1.1 Effect of Mechanical (Static) Load pressure

The effect of the load on the crack surface for three crack cases is summarized as shown below.

1. Crack Extension simulations

Crack tip Maximum principal stress

The first simulation was conducted in XFEM by increasing the crack length with 0.25 mm amount and see the increment of the crack tip principal stress. For example, let's have a look on three cases of crack lengths i.e 5, 8 and 10mm.

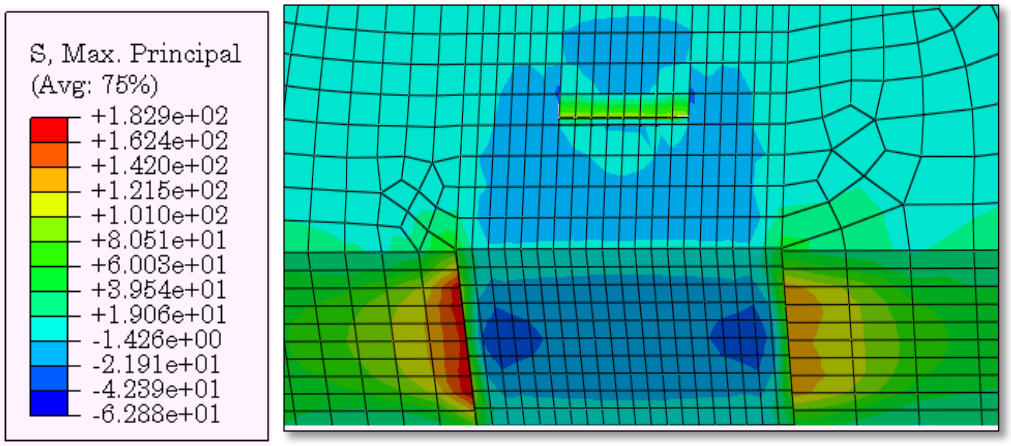

Figure 4.1: Crack tip Maximum principal stress (MPa) of 5mm crack

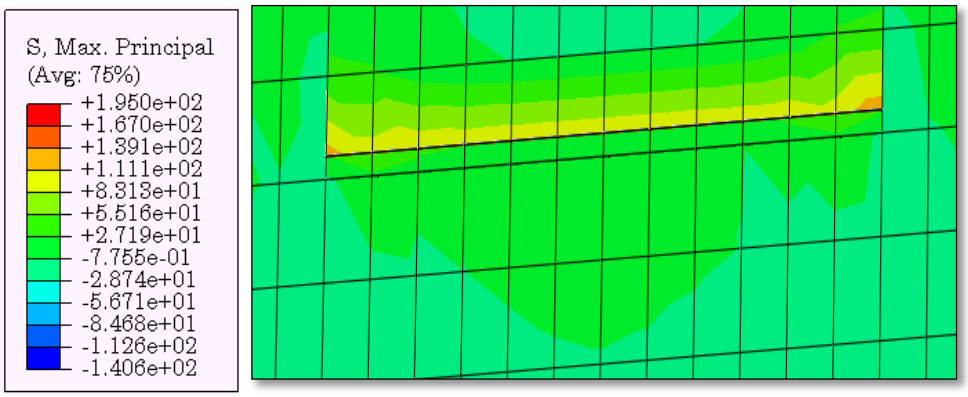

Figure 4.2: Crack tip Maximum principal stress (MPa) of 8 mm crack

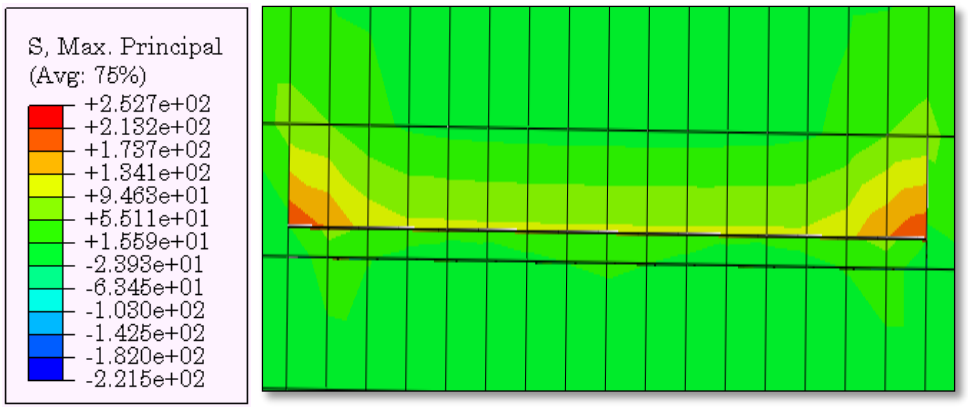

Figure 4.3: Crack tip Maximum principal stress (MPa) of 10 mm crack

Crack tip Equivalent Plastic strain (PEEQ)

There is a higher Plastic strain at the midpoint section of the crack surface.

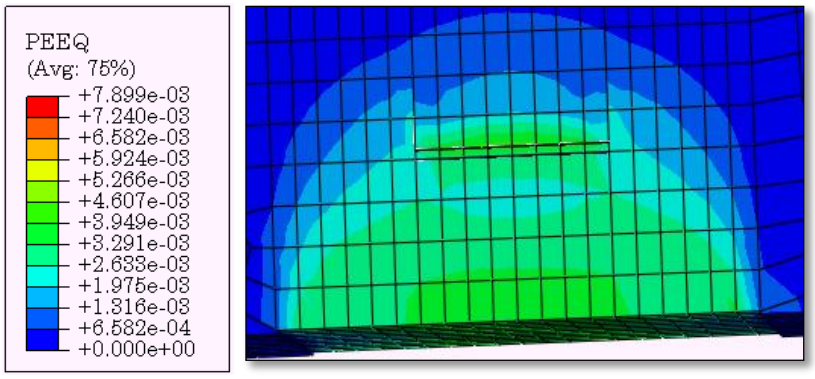

Figure 4.4: Crack tip Equivalent Plastic strain of 5mm crack

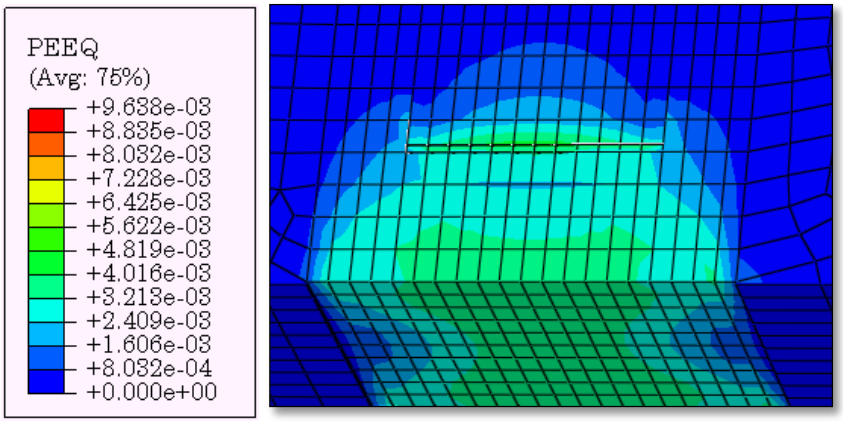

Figure 4.5: Crack tip Equivalent Plastic strain of 8mm crack

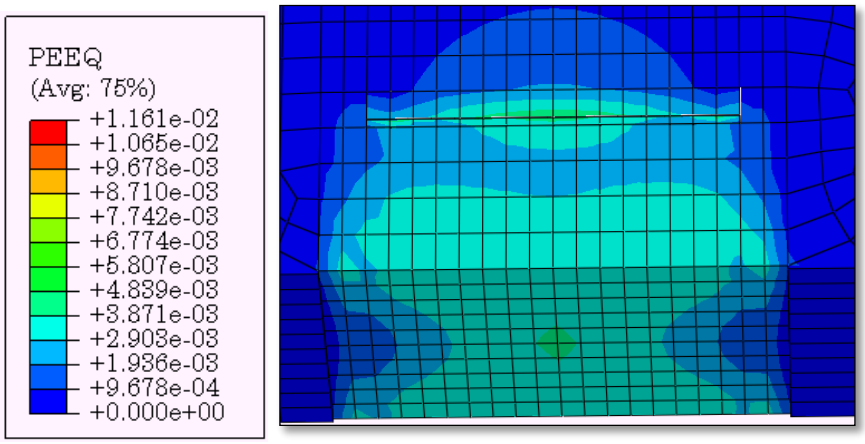

Figure 4.6: Crack tip Equivalent plastic strain of 10 mm crack

2. Simulation at Different crack orientations

Crack tip Maximum principal stress

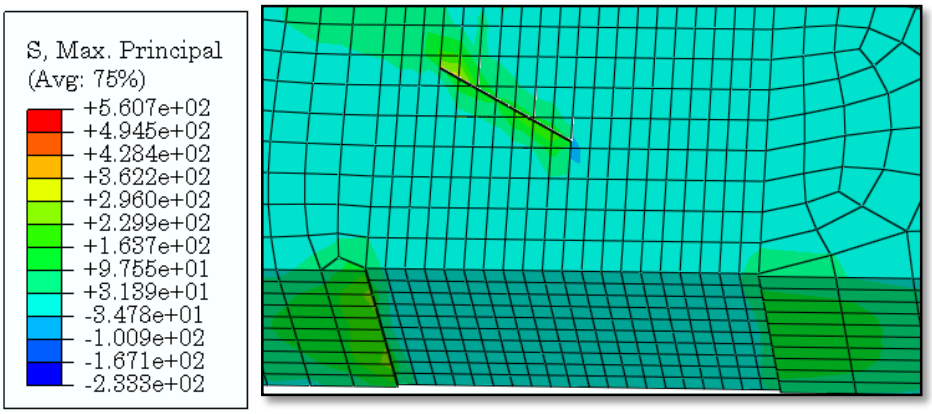

Figure 4.7: Maximum principal stress (MPa) for 5mm-30^0 crack

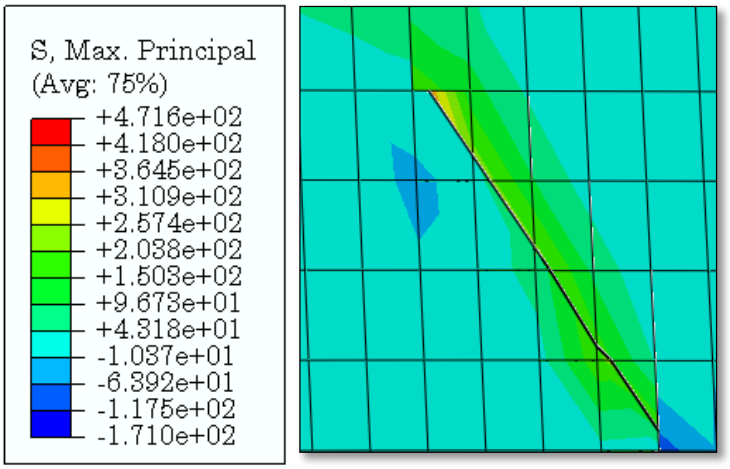

Figure 4.8: Maximum principal stress (MPa) for 5mm-60^0 crack

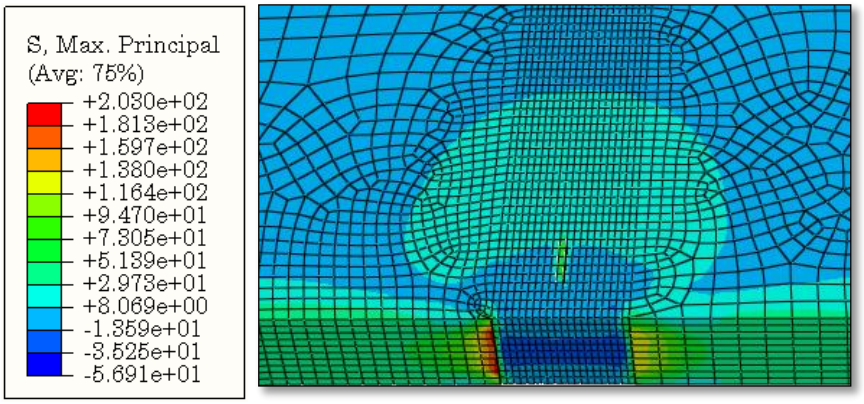

Figure 4.9: Maximum principal stress in MPa for 5mm-90^0 crack

Crack tip Equivalent Plastic Strain (PEEQ)

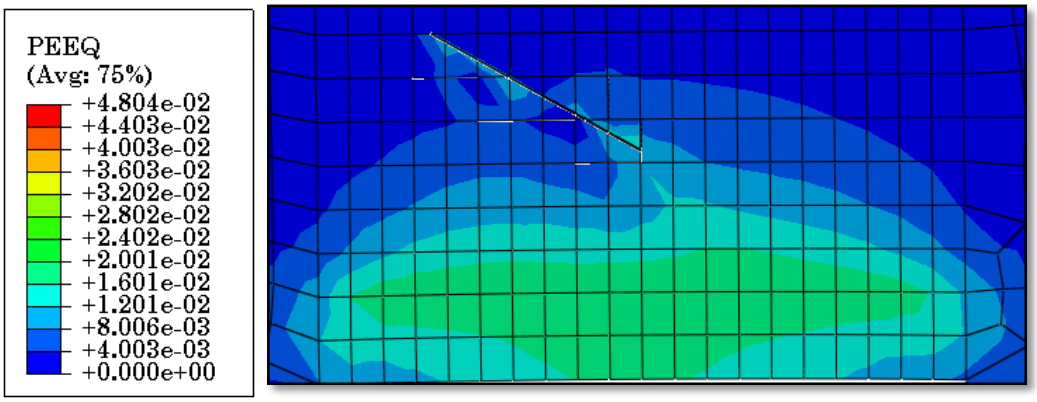

Figure 4.10: Equivalent plastic strain of 5mm-30^0 crack

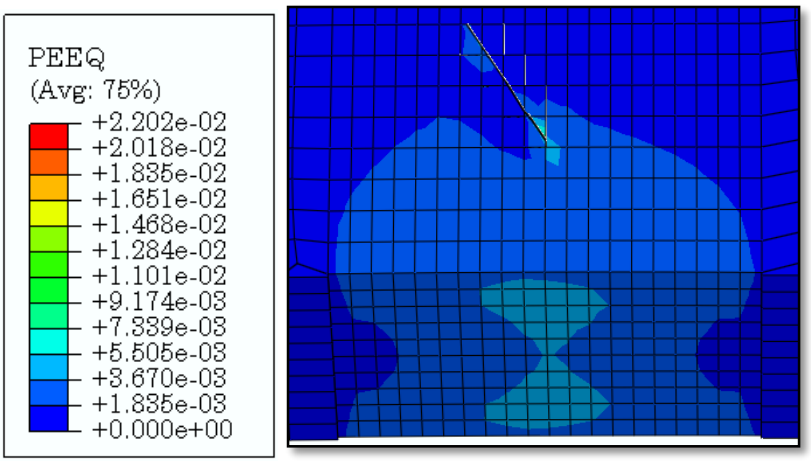

Figure 4.11: Equivalent plastic strain of 5mm-60^0 crack

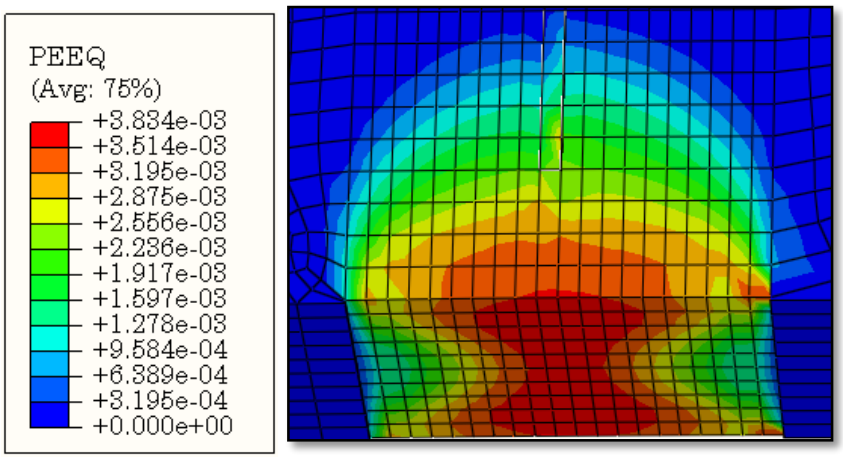

Figure 4.12: Equivalent plastic strain of 5mm-90^0 crack

4.1.2 Combined Effect of Frictional Heating Temperature and Mechanical load

1. Crack Extension Simulations

Crack tip Maximum principal stress

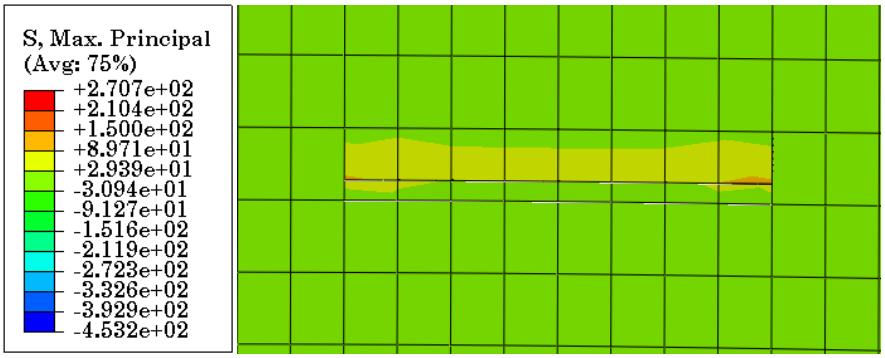

Figure 4.13: Crack tip Maximum Principal Stress (MPa) of 5mm crack

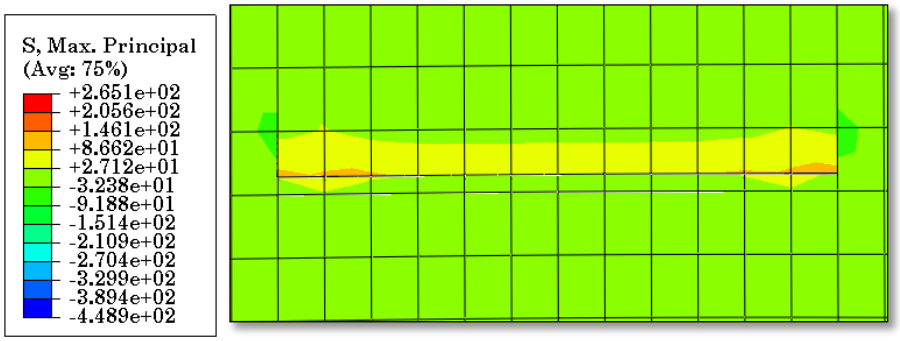

Figure 4.14: Crack tip Maximum principal stress (MPa) of 8mm crack

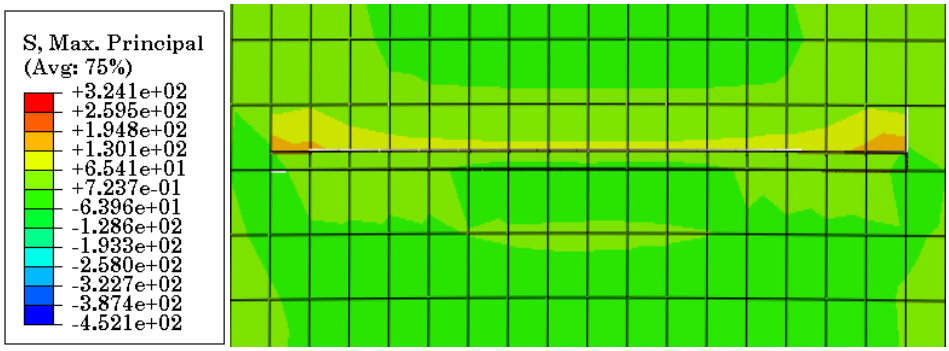

Figure 4.15: Crack tip Maximum principal stress (MPa) of 10mm crack

Crack tip Equivalent plastic strain(PEEQ)

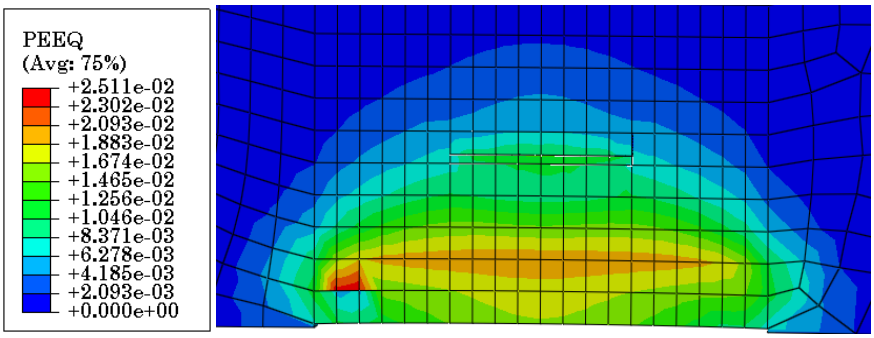

Figure 4.16: Crack tip Equivalent plastic strain of 5mm crack

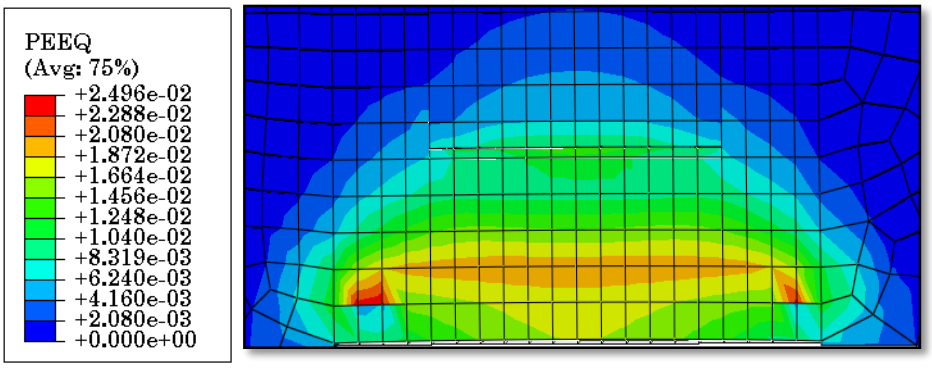

Figure 4.17: Crack tip Equivalent plastic strain (PEEQ) for 8mm crack

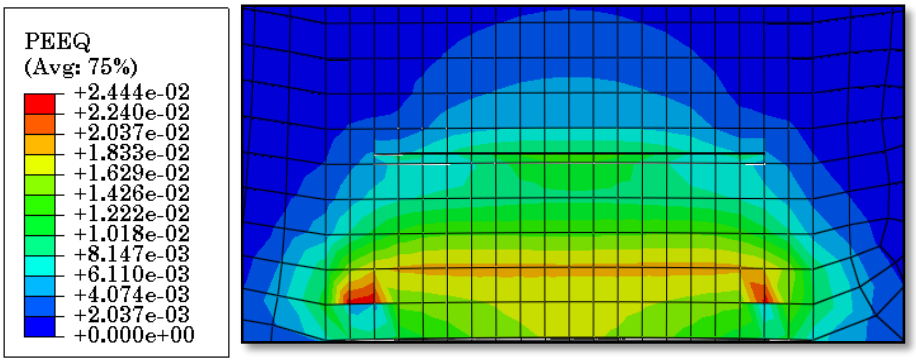

Figure 4.18: Crack tip Equivalent plastic strain for 10 mm crack

2. Simulation of Different crack orientations

Crack tip Maximum principal stress

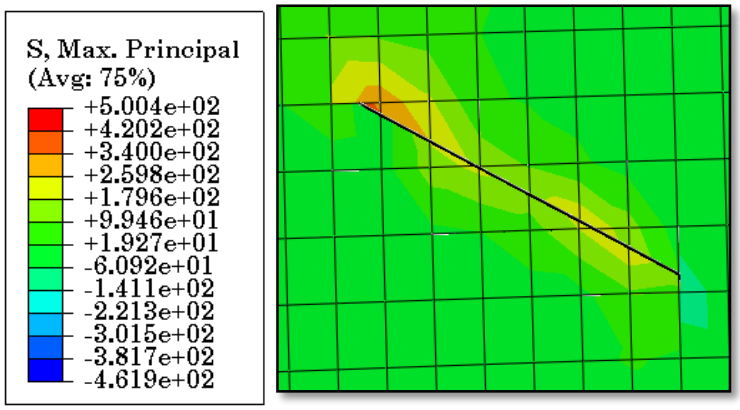

Figure 4.19: Maximum principal stress (MPa) for 5mm-30^0 crack

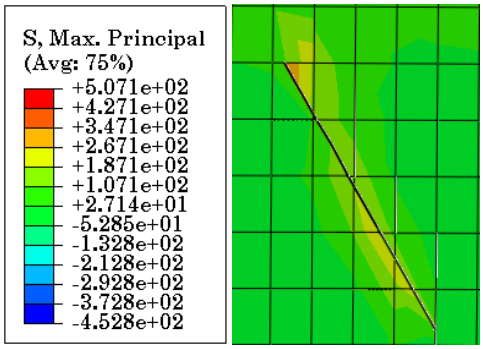

Figure 4.20: Maximum principal stress of 5mm-60^0 crack

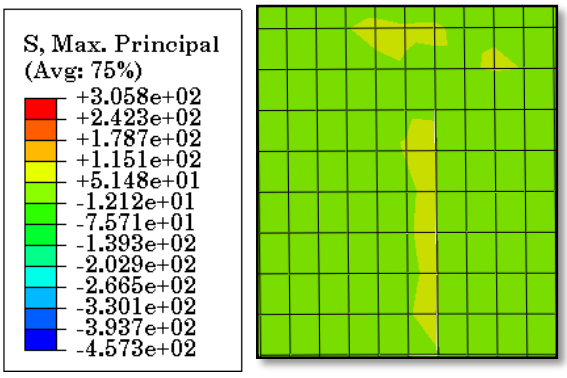

Figure 4.21: Maximum principal stress of 5mm-90^0 crack

Crack tip Equivalent plastic strain (PEEQ)

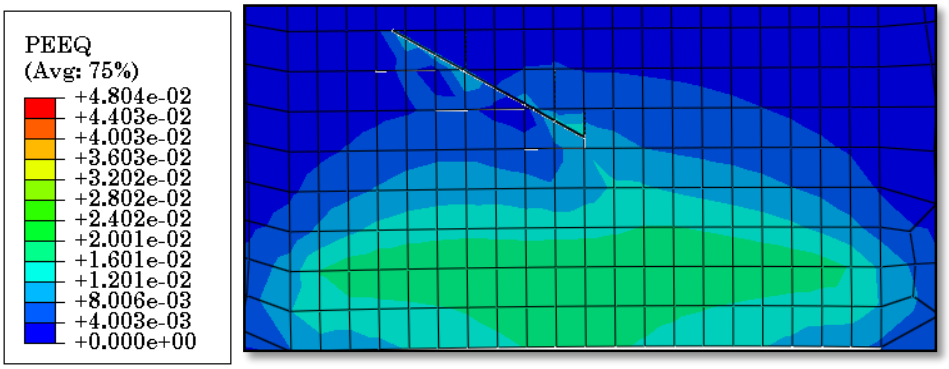

Figure 4.22: Equivalent plastic strain for 5mm-30^0 crack

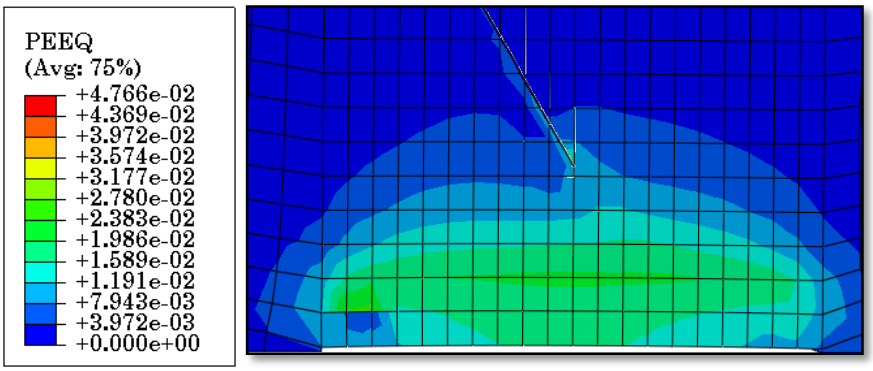

Figure 4.23: Equivalent plastic strain for 5mm-60^0 crack

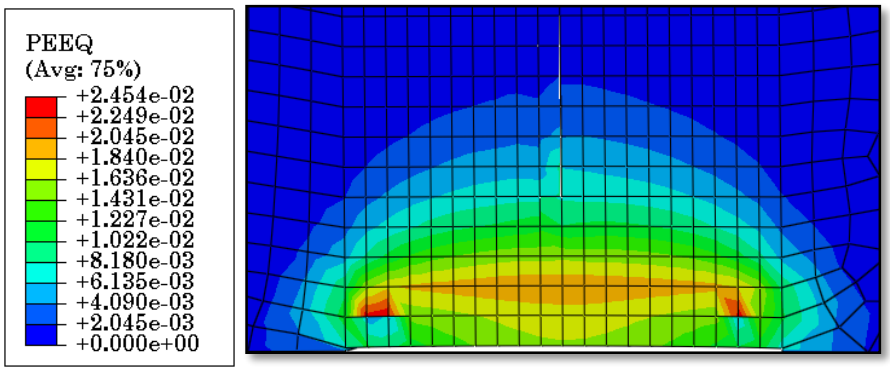

Figure 4.24: Equivalent plastic strain for 5mm-90^0 crack

The mechanical and combined load simulation results can therefore can be summarized as follows:

Table 4.1: XFEM crack tip principal stress versus Crack Extension

Load	Mechanical load	Thermo-Mechanical
Crack Length (mm)	Crack surface Principal stress, MPa	
1	20	21
1.25	20.8	22.8
1.5	21	23.9
1.75	21.5	25.1
2	21.9	26.3
2.25	22.4	27.4
2.5	31	35
2.75	34.2	44
3	38.5	53.3
3.25	46.4	74.5
3.5	55	81
3.75	73	89.3
4	84.6	107
4.25	99.7	121
4.5	105	139
4.75	112	143
5	121.5	150
5.25	125	154
5.5	132	161
5.75	140	166
6	148	171
6.25	153	178
6.5	158	184
6.75	161	190
7	163	198
7.25	164	200
7.5	165	202
7.75	166	204
8	167	205.6
8.25	172	208.1
8.5	181	211.3
8.75	190	221
9	201	229.2
9.25	218	237
9.5	223	245
9.75	238	251
10	252.7	268.6

Table 4.2: Maximum principal stress versus crack inclination angle

	Mechanical Load	Thermo-Mechanical
Crack inclination angle, θ	Principal stress at the crack tip, MPa	
10	205	206.1
15	227.9	230.3
30	296	340
45	312.4	392.6
60	364.5	427.1
75	192	127.6
90	116.4	115.1

Table 4.3: Crack tip equivalent plastic strain versus crack extension

Crack length (mm)	**Equivalent Plastic deformation, mm**	
	Mechanical Load	Thermo-mechanical
1	0.000978	0.00345
1.25	0.00112	0.00398
1.5	0.00127	0.00423
1.75	0.00144	0.00467
2	0.001678	0.00506
2.25	0.00188	0.00545
2.5	0.00214	0.00584
2.75	0.00239	0.00623
3	0.00255	0.00662
3.25	0.00272	0.00701
3.5	0.00301	0.00739
3.75	0.00314	0.00779
4	0.00327	0.00818
4.25	0.00349	0.00857
4.5	0.00364	0.00896
4.75	0.00379	0.00916
5	0.00395	0.009356
5.25	0.00401	0.00964
5.5	0.0041	0.0103
5.75	0.00423	0.0107
6	0.00432	0.0112
6.25	0.00443	0.0115

6.5	0.00452	0.012
6.75	0.00461	0.0127
7	0.00468	0.01298
7.25	0.00472	0.01325
7.5	0.00479	0.01387
7.75	0.0048	0.014
8	0.00488	0.01456
8.25	0.00497	0.01471
8.5	0.00517	0.01487
8.75	0.00531	0.01492
9	0.00541	0.01499
9.25	0.00546	0.015
9.5	0.00554	0.01505
9.75	0.00564	0.0151
10	0.00581	0.01512

4.2 Discussion

In the Abaqus XFEM, a skidded wheel model under combined load of Mechanical and Temperature at the surface with different initial crack lengths and crack inclination angles were simulated. Since the TAZ (Temperature Affected Zone) is very small in the simulation, therefore it cannot increase the stress concentration around the crack surface which is at the depth of 5mm from the surface.

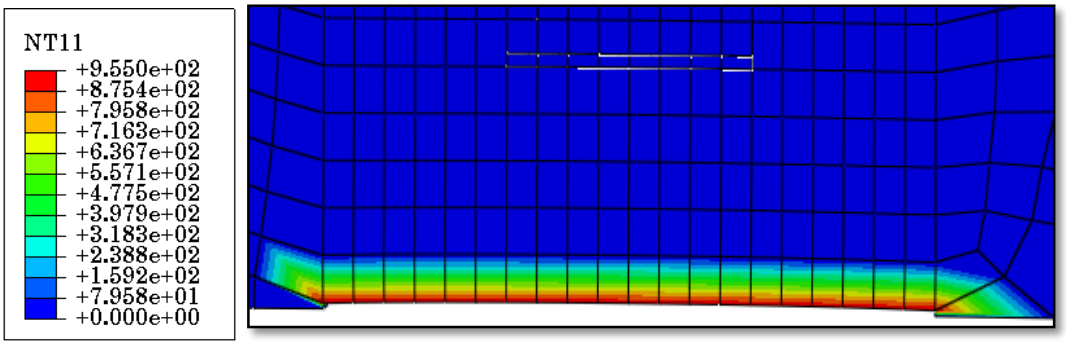

Figure 4.25: Depth of the temperature distribution (^{0}C)

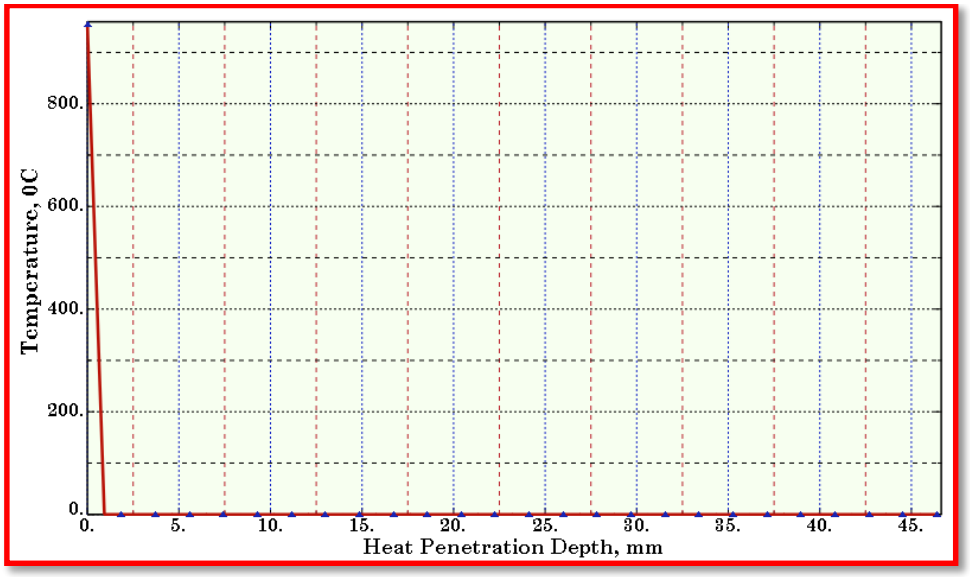

Figure 4.26: Temperature vs. Penetration depth

The maximum level of the stresses and plastic strain are below the crack surface i.e below 5mm to break a crack bond for propagation. The stress with and without a temperature has a small significant change to the mechanical load stress. This is according to the prediction of the Peclet's number for a high sliding velocity motions in Chapter 4.

From Figure 4.26, we can infer that as the crack extends the crack tip principal stress also increases and as the crack grows the wheel will lose integrity due to stress accumulation at the surface. We can approximate using 4th order polynomial curve of $y=16z^4-3z^3-49z^2+82z+160$ where $z=\frac{(x-5.5)}{2.7}$ with a maximum of approximately Relative error (E_r)=12 of residual error in the fitting.

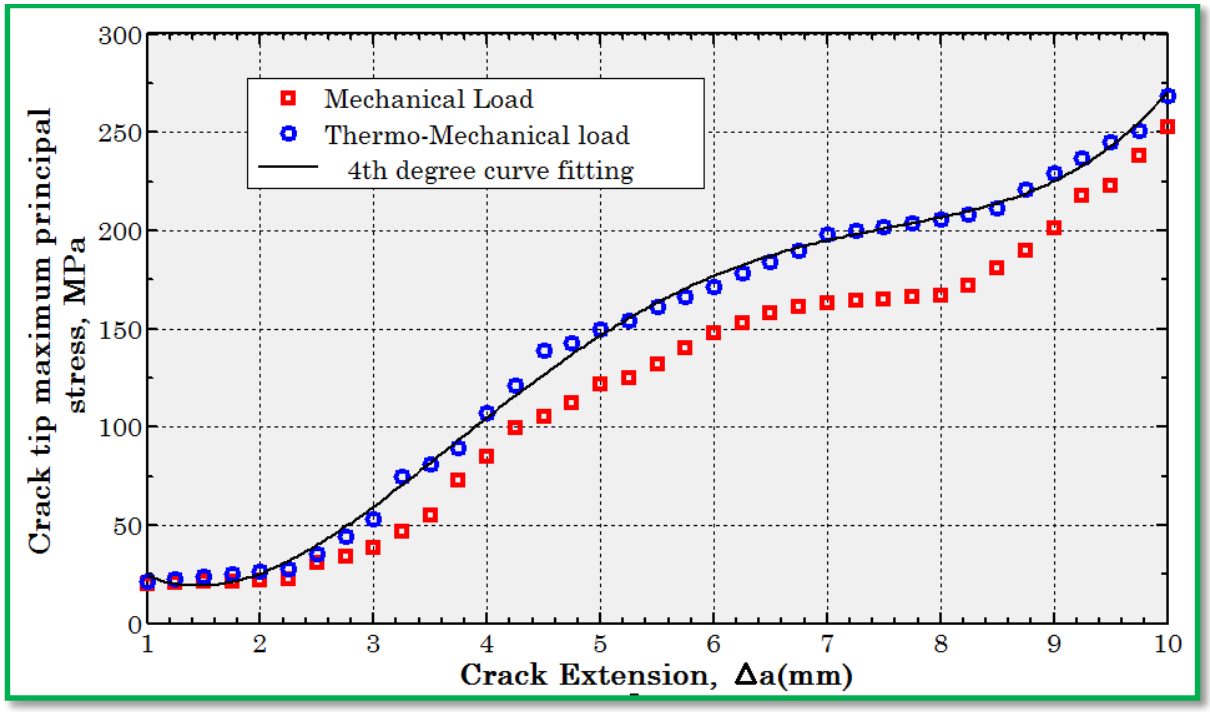

Figure 4.27: Crack tip principal stress versus Crack Extension (Δa)

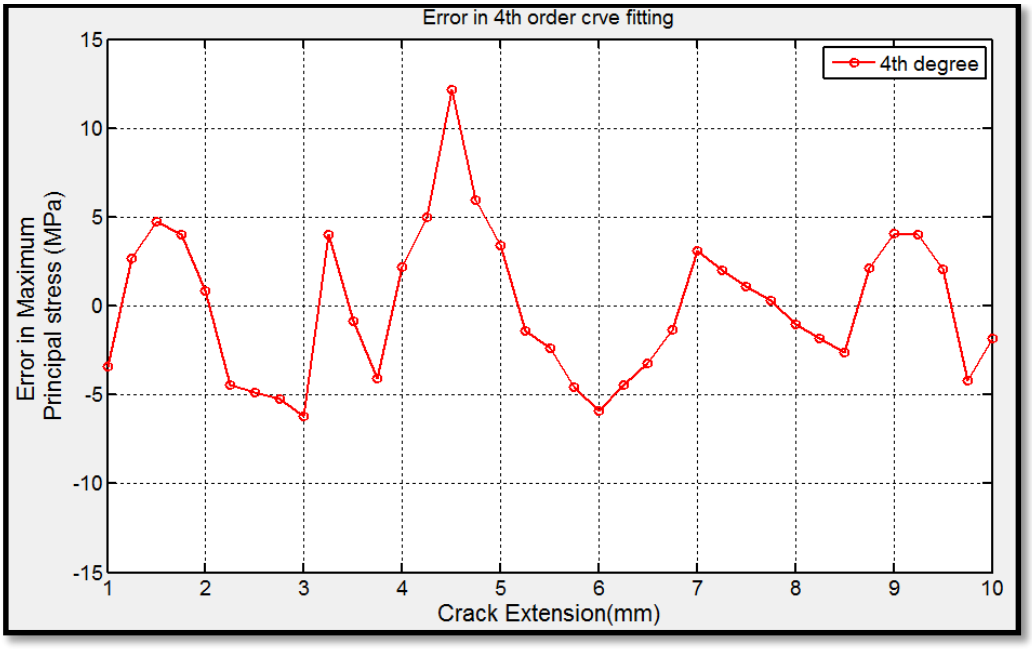

Figure 4.28: Residual Error of the XFEM MAXPS and 4th order curve fitting

The crack tip equivalent plastic strain (PEEQ) seems increasing with a cubic polynomial function scheme according to the curve fitting equation of -0.000019x^3+0.00026x^2+0.0005x+0.0031.

The plastic deformation of the wheel will also increase as the crack grows. And in the case of PEEQ case the combined thermal and mechanical loading will show relatively large deformation amount than the mechanical (static) load.

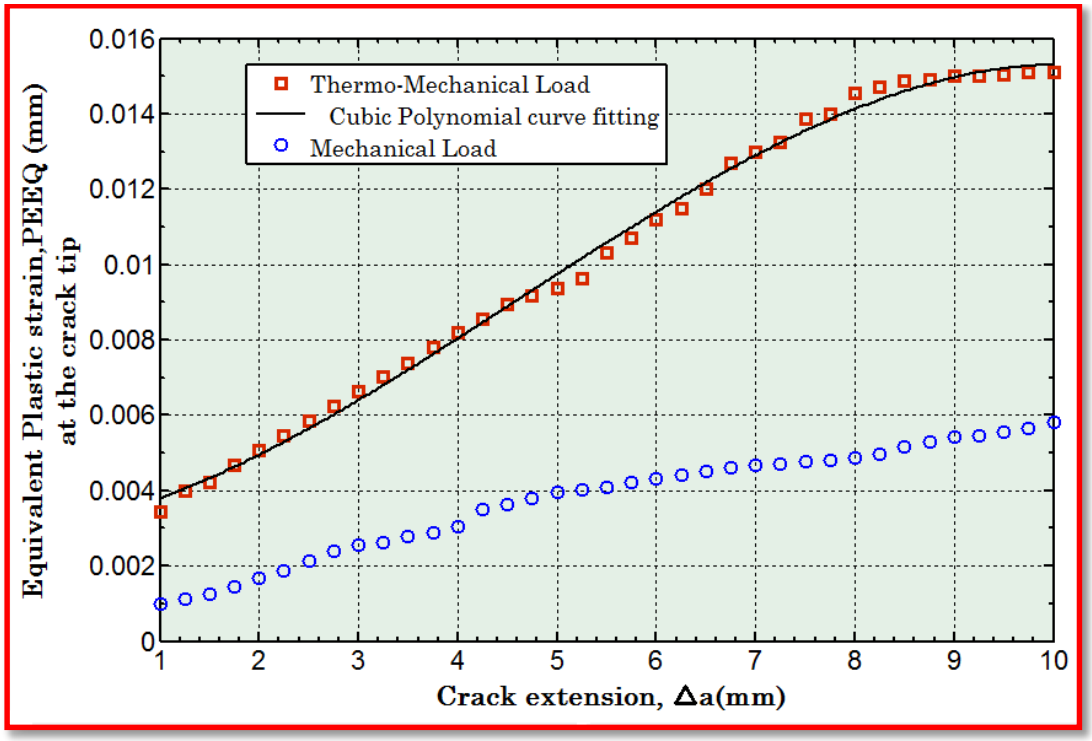

Figure 4.29: Equivalent Plastic strain (PEEQ) versus Crack Extension (Δa)

The observed result can be approximated using third order polynomial approximation with a relatively low error level as it can be seen in Figure 4.29.

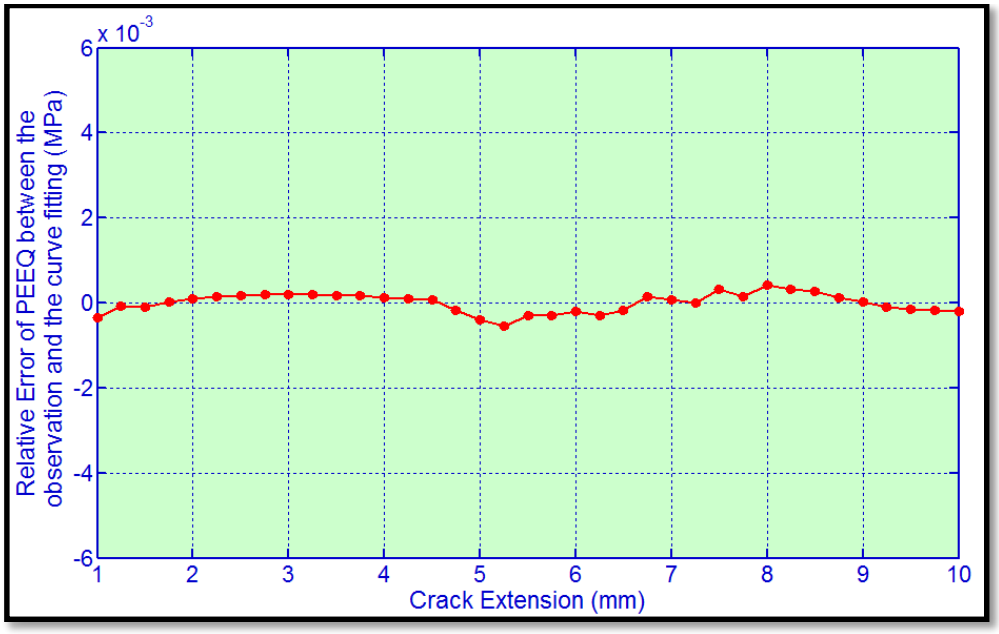

Figure 4.30: Residual error in curve fitting the PEEQ curve versus Crack extension

The maximum crack tip principal stress and crack inclination angle shows that the 60^0 inclined shows maximum value and more over Vertical cracks are less likely to increase crack length.

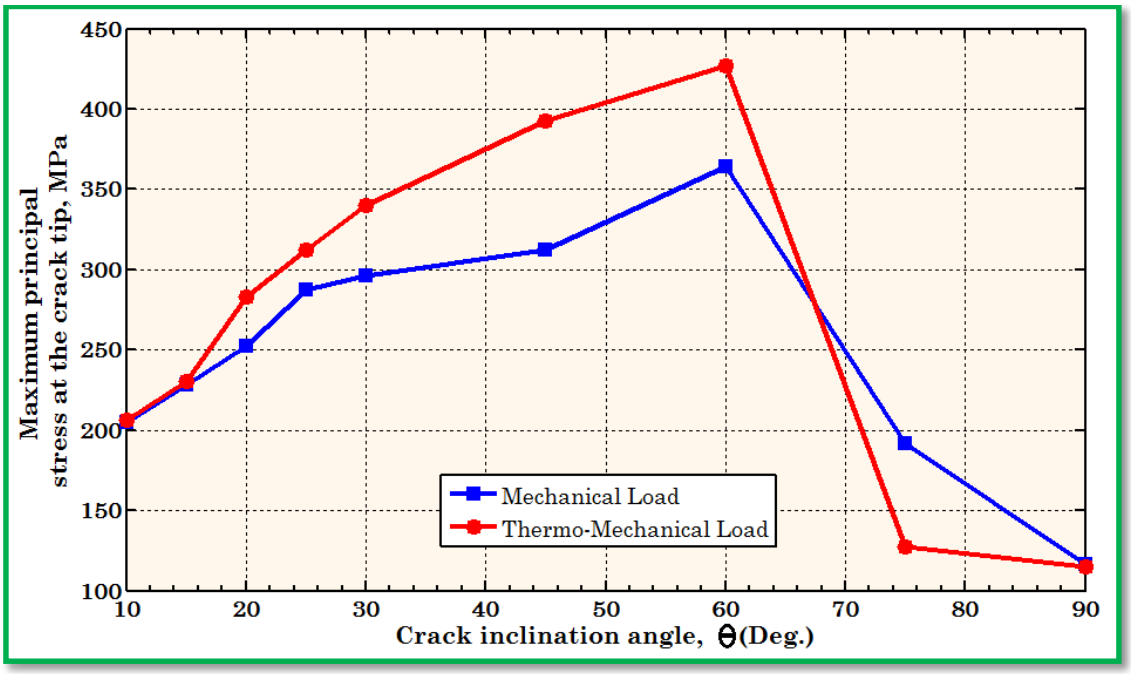

Figure 4.31: Crack tip principal stress versus Crack inclination angle

Chapter Five

Conclusion and Recommendations

5.1 Conclusion

This thesis goes through a crack growth simulation of wheel having a flat subsurface crack and that skids along a rail to check the effect of the additional frictional heat induced while skidding beside the normal static mechanical load imposed on it for the crack propagation length and stress distribution schemes using a method of Extended Finite Element Method (XFEM) in Abaqus for a safety critical concerns. The wheel is modeled as an Elastic-Plastic material and isotropic hardened. The wheel which was considered is skating on the rail to have a temperature rise of 955 ^{o}C.

Extended finite Element Method (XFEM) in recent years become an efficient method to analyze crack propagation problems without the need to modify the mesh generated successively but it has some limitations. And the results obtained are physically similar with FEM results previously done.

5.2 Recommendations

Crack propagation is a complex and high cycle process but a serious problem of materials and components and should be prevented timely through periodic check-ups and following maintenance issues concerning the components subjected to cracks. Based on the study results the following recommendations are prominent for future studies:

- Modeling of crack based on dynamic loading conditions (Rolling Fatigue loads) for a longer duration of simulation time is advisable for the effectiveness of the prediction of the status of the cracks for the future.
- Since sharper and edge cracks are resistive for propagation elliptical cracks should be considered beside the above mentioned suggestion.
- Studying Cracks at different depths and orientations can be helpful for the prediction of different crack characteristics efficiently.
- Linearized pressure consideration may alter the result in consideration of the tri-axially distribution of stress therefore efficient contact geometry modeling should be applied to get accurate results.
- For the purpose of addressing the material property, different material modeling's should be considered to see the effect of the results variation.
- As the solution of XFEM is mesh dependent, study on the effect of mesh refinement should be considered.

For the Railway service firms:

- Malfunctioning of brakes should be checked periodically for the possible option of crack arresting.
- Should determine which cracks can propagate faster so that can cause abrupt wheel failure based on the above specified suggestions.

5.3 Future Research Directions

During the overall evolution of this thesis work, some research gaps in the area of modeling cracks for railway applications are observed. Some of the gaps that should be filled are:

- Modeling of wheel cracks under 'Fully coupled Mechanical and thermal stresses' (i.e the thermal load is fully dependent on the mechanical applied load on the cracked system) of the mating surfaces i.e wheel and rail in XFEM. As per the future Abaqus and LS-Dyna XFEM capabilities.

- Modeling of crack propagation under Dynamic (Running) conditions using XFEM
- Effect of running conditions like Curving, Hunting and Bouncing of railway car on the crack propagation of the wheel cracks.
- Experimental validation of the thermal heat flux effect on the subsurface and surface defects of a railway wheel and rail.
- Effect of material hardening on the fracture property of the wheel- Towards Experimental validation.

Bibliography

[1]. Norihisa Tadakoshi and Takao Okamoto, Rail Transport in the world's Major cities, October 2000, Japan.

[2]. UNECA, Africa Review Report on Transport, United Nations Economic and Social council 27-30, October 2009, Addis Ababa, Ethiopia.

[3]. Club Feroviar conferences, Railway Passenger transport in the Sustainable mobility agenda, Sibuiu Technical-Scientific colloquium II edition, March 2012.

[4]. Zx liu and H.C Gu, Failure modes and Materials performance of Railway wheels, ASM international, Journal of Materials Engineering and Performance, Vol 9, May 2000.

[5]. N.A. Akeel et al, Analysis of RCF damage initiation at the wheel-Rail interface, Australian Journal of Basic and applied sciences 937-945, 2011, Selangor, Malaysia.

[6]. Yongming Liu, Liming Liu and Sankaran Mahaderan, Analysis of subsurface crack propagation under Rolling contact loading in Railroad wheels using FEM, Engineering Fracture mechanics, 2659-2674, 74(2007).

[7]. R. Roberti *et al,* on the crack path of RCF cracks in a railway wheel steel, Italy.

[8]. Adam Bevan et al, Development and validation of a wheel wear and rolling contact fatigue damage model, University of Huddersfield, Institute of Railway Research, 2013, UK.

[9]. A. Ekberg, E. Kabo, H. Anderson, Predicting Fatigue life of railway wheels, 13th International wheel set congress, Rome Italy, September 19-21, 2001.

[10]. Nagvendra Kumar kanoje, Satish C.Sharma, S.P.Harsha, EPFM analysis of subsurface crack beneath a wheel flat using dynamic condition, Procedia Materials science 6 (2014) 43-60.

[11]. Venkata Sasidher Sura;Failure Modelling and Life Prediction of Railroad wheels;PhD thesis; Vanderbilt University, Nashville, Tennessee, December 2011.

[12]. S.Caprioli, T.Vernersson, A.Ekberg, Thermal cracking of a railway tread due to Tread braking- Critical crack sizes and influence of Repeated thermal cycles,

[13]. National Aeronautics and Space Administration (NASA), System Failure case studies DERAILED, Volume I issue 5, March 2007.

[14]. Roya sadat Ashofteh and Ali Mohammadnia, Stress analysis in the Elastic-Plastic Analysis of Railway wheels, International journal of Railway, vol 7, March 2014.

[15]. Krste Cvetkovski, Influence of thermal loading on mechanical properties of railway wheel steels, PhD thesis, Chalmers university of Technology, Gothenburg, Swededn, 2012.

[16]. S.Caprioli, T.Vernersson, A. Ekberg; Thermal cracking of a Railway wheel Tread due to Tread Braking-Critical crack sizes and Influence of Repeated Thermal cycles; CHARMEC, Gothenburg, Sweden. 28

[17]. Azadeh Haidari, Parisa Hosseini Tehrani; Thermal load effects on Fatigue life of a cracked railway wheel; Latin America Journal of Solids and Structures, 12 (2015) 1144-1157.

[18]. Mundissa; Investigation of surface Ratcheting due to Rail/Wheel contact, PhD thesis.

[19]. J.J Kalker; Wheel-Rail Rolling Contact theory; Wear, 144(1991) 243-261; Netherlands.

[20]. Zwierczyk, Peter Tamas, Thermal and Stress analysis of a railway wheel-rail Rolling-sliding contact, PhD Dissertation, Budapest University of Technology and Economics, Budapest, 2015.

[21]. Ulf olofsson and Roger Lewis, HandBook of Railway vehicle Dynamics (Tribology of the wheel-Rail contact), Taylor&Francis Group LLC, 2006. 60

[22]. W.Yan, F.D. Fischer, Applicability of the Hertz Contact theory to Rail-wheel contact problems, Applied Mechanics 70(2000) 255-268, Springer-Verlag, 2000. 59

[23]. Matin Shahzamanian Sichani, Wheel-Rail Contact Modelling in Vehicle Dynamics Simulation, Licentiate Thesis, KTH Engineering Science, Stockholm, Sweden, 2013. 58

[24]. Radu Popovici; Friction in wheel-Rail; PhD Thesis; University of Twente, February 2010.

[25]. M.Wallentin, H.L.Bjarnehed, R.Lunden; Cracks around railway wheel flats exposed to rolling contact loads and residual stresses; Wear 258 (2005) 1319-1329. 66

[26]. Andreas Heckmann, Alexander Keck, Ingo Kaiser, Bernard Kurzeck; The Foundation of the DLR Railway Dynamics Library: the wheel-Rail contact, Proceedings of the 10th International Modelica conference, March 10-12, Lund, Sweden, 2014.

[27]. Harmen Blok, Institution of mechanical Engineering, 2, 222 (General discussion on Lubrication).

[28]. J.C. Jaeger, Moving sources of Heat and The temperature at sliding contacts, October 7, 1942.

[29]. J.R. Barber, Distribution of Heat between sliding surfaces, Journal mechanical Engineering science, vol.9, No.5, 1967.

[30]. B.A. Sherwood and W.H. Bernard, Work and heat transfer in the presence of sliding friction, American association of Physics Teachers 52(11), November 1984.

[31].K.Knothe, S.Liebelt, Determination of temperatures for sliding contact with application for wheel-rail systems, Wear 189 (1995) 91-99.

[32]. V.Gupta, G.T.Hahn, P.C.Bastias and C.A.Rubin, Calculations of the frictional heating of a locomotive wheel attending rolling plus sliding, wear 191(1996) 237-241.

[33]. F.D.Fischer, E.werner, W.Y.Yan, Thermal stresses for frictional contact in wheel-rail systems, wear 211(1997) 156-163 September, Lisbon, Austria.

[34]. Martin Ertz and Klaus Knothe, A comparison of analytical and numerical methods for the calculation of temperatures in wheel/rail contact, wear 253(2002) 498-508.

[35]. M.Ertz, K.Knothe; Thermal stresses and shakedown in wheel/rail contact; Springer, 2003 715-729, Verlag 2003.

[36]. Martin Ertz, Klaus Knothe; A Comparison of analytical and Numerical methods for the calculation of temperature in wheel/rail contact, wear 253 498-508, August 2002, Germany.

[37]. S.S Deshpande, S.Srikari, V.K.Banthia, K.Jagadeesh, N.Chowdhary; Investigation of Effects of Different Braking Systems on Rail wheel spalling; SAS Tech Journal, Volume 9, Issue 2, September 2010.

[38]. T.L. Anderson, Fracture Mechanics: Fundamentals and Application 3rd Edition, Taylor and Francis group, 2005.

[39]. Majid Mirzaei, Fracture Mechanics: Theory and Applications-Lecture notes, TM university.

[40]. Samrawit Addis, Analysis of crack propagation in rotating composite Disc, MSc. Thesis, Addis Ababa university, 2010.

[41]. N.K. Simha, F.D. Fischer, G.X. Shan, C.R.Shan, C.R.Chen, O.Kolednik, J-integral and crack driving force in elastic-plastic materials, Journal of Fracture Mechanics and Physics of solids 56(2008) 2876-2895.

[42]. Krishna Lok Singh, Kamal Keswani and Mallikarjun Vaggar, Crack growth simulation of stiffened fuselage panels using XFEM techniques, Indian Journal of Engineering and Materials science (Vol.2), August 2014, 418-428.

[43]. Awas Ahmed, Extended Finite Element Method (XFEM)-Modeling arbitrary discontinuous and failure analysis, MSc thesis, University of studi da Pavia, April, 2009.

[44]. Dibakar Datta, Introduction to Extended Finite Element (XFEM) Method, Erasmus MSc in computational mechanics (No: 080579k), France.

[45] Chao Zhang, Peng Cao, Yixiang Cao, Jianbo Li, Using Finite Element software to simulation Fracture Behaviour of Three-point Bending Beam with Initial crack, Journal of software, Vol.8, No.5, May 2013.

[46]. Vineet Kumar, Indra Vir Singh, Bhanu Mishra, XFEM, Crack Growth Examination of Cryo-Rolled (CR) 6082 Al alloys, International Journal of Emerging Technology and Adavced Engineering (Vol.4) Special Issue 1, February 2014.

[47]. Zhen-Zhong Du, Extended Finite Element Method (XFEM) in Abaqus, Dessault system simulia.

[48]. Ted Belytschenko, Robert Gracie, Giulio Ventura, A review of Extended/Generalized finite element Methods for Material modelling.

[49]. E.Giner, N.Sukumar, J.E. Tarancon, F.J. Fuenmayor, An Abaqus implementation of the Extended finite element method, Engineering Fracture Mechanics, October 24, 2008,22.

[50]. Jay Sepheri, Application of Extended Finite Element (XFEM) to simulate Hydraulic Fracture Propagation from Oriented Perforations, MSc. Thesis1 Texas Tech university, May 2014.

[51]. Hao Wang and Jian Wang, Numerical analysis of surface crack propagation in Flexible Pavements using XFEM and Cohesive Zone Model, International Journal of Pavement research and Technology 7(3), 178-184, May 2014.

[52]. Chao Zhang, Peng Cao, Yixiang Cao, Jianbo Li, Using Finite Element software to simulation Fracture Behaviour of Three-point Bending Beam with Initial crack, Journal of software, Vol.8, No.5, May 2013.

[53]. M.Kracalik, W.Daves, T.Antretter, Calculation of crack driving forces of surface cracks subjected to rolling/sliding contact, Engineering Fracture Mechanics 152 (2016) 10-25.

[54]. Dessault systems, Abaqus Manual, 2012.

[55]. D.Peng, R.Jones, T.Constable, A study into crack growth in a railway wheel under thermal stop brake loading spectrum, Engineering Failure Analysis 25 (2012) 280-290.

[56]. Sara Caprioli, Short rolling contact fatigue and thermal cracks under frictional rolling-A comparison through simulations, Engineering Fracture Mechanics 141(2015) 260-273.

[57]. Lei Wu, Zefeng Wen, Wei Li, Xuesong Jin, Thermo-elastic-plastic finite element analysis of wheel/rail sliding contact, Wear 271(2011) 437-443.

[58]. Sara caprioli, Tore Vernersson, Kazuyuki Handa, Katsuyoshi Ikeuchi, Thermal cracking of railway wheels: Towards experimental validation.

[59]. Ethiopian Railway corporation (ERC), E-W Line Project, China Railway Group limited (2009).

[60]. Brown University, Abaqus Tutorial for Advanced Mechanics of Solids. http://www.engin.brown.edu/courses/En175/Abaqustut.htm.

[61]. Siva Naga Venkata Ravi Kiran Kurapati, Elastic-plastic indentation deformation in Homogenous and Layered materials: Finite Element Analysis, University of Kentuky Master's Thesis, 2008.

[62]. Jonathan Mullins and Jens Gunnars, Influence of Hardening Model on Weld residual stress Distribution, Swedish Radiation safety Authority, 2009.

[63]. Hibbit, Karlsson and Sorenssen, Inc, ABAQUS/Post Manual, Version 5.8, Pawtucket, RI, USA 1999.

[64]. Nicholas Szwaja, Elastic, and Elastic-plastic Finite Element Analysis of a Tension Test specimen with and without voids, Rensselaer Polytechnic Institute MSc. Thesis, Hartford, Connecticut, August 2012.

[65]. Richard G.Budynas, J.Keith Nisbett, Mechanical Engineering design (9th Edition), Mc-Graw Hill companies, New York, 2011.

APPENDIX A

HERTZ COMPUTATIONAL CONSTANTS

Ψ	n_a	n_b	n_p	n_δ	Ψ	n_a	n_b	n_p	n_δ
0.01923	1.013	0.9873	0.9999	0.9999	**0.7238**	1.979	0.5938	0.8507	0.8451
0.03949	1.027	0.9742	0.9997	0.9997	**0.7449**	2.053	0.5808	0.8386	0.8320
0.06087	1.042	0.9606	0.9992	0.9992	**0.7673**	2.141	0.5665	0.8246	0.8168
0.08350	1.058	0.9465	0.9985	0.9985	**0.7911**	2.248	0.5505	0.8082	0.7990
0.1075	1.076	0.9318	0.9974	0.9974	**0.8166**	2.381	0.5325	0.7887	0.7775
0.1330	1.095	0.9165	0.9960	0.9960	**0.8300**	2.463	0.5224	0.7774	0.7650
0.1602	1.117	0.9005	0.9942	0.9942	**0.8441**	2.557	0.5114	0.7647	0.7509
0.1894	1.141	0.8873	0.9919	0.9919	**0.8587**	2.669	0.4993	0.7504	0.7349
0.2207	1.168	0.8660	0.9890	0.9889	**0.8741**	2.805	0.4858	0.7338	0.7163
0.2545	1.198	0.8472	0.9853	0.9852	**0.8904**	2.975	0.4704	0.7144	0.6943
0.2913	1.233	0.8271	0.9805	0.9804	**0.9077**	3.199	0.4524	0.6909	0.6675
0.3314	1.274	0.8056	0.9746	0.9744	**0.9113**	3.253	0.4484	0.6856	0.6613
0.3755	1.322	0.7822	0.9669	0.9667	**0.9150**	3.311	0.4442	0.6799	0.6549
0.4245	1.381	0.7565	0.9571	0.9566	**0.9187**	3.373	0.4398	0.6740	0.6481
0.4795	1.456	0.7278	0.9440	0.9432	**0.9225**	3.441	0.4352	0.6678	0.6409
0.4914	1.473	0.7216	0.9409	0.9400	**0.9264**	3.514	0.4304	0.6612	0.6333
0.5036	1.491	0.7152	0.9376	0.9366	**0.9303**	3.594	0.4253	0.6542	0.6251
0.5161	1.511	0.7086	0.9340	0.9329	**0.9342**	3.683	0.4199	0.6467	0.6164
0.5291	1.532	0.7019	0.9302	0.9290	**0.9383**	3.781	0.4142	0.6387	0.6071
0.5423	1.554	0.6949	0.9262	0.9248	**0.9425**	3.890	0.4080	0.6300	0.5970
0.5560	1.578	0.6876	0.9219	0.9203	**0.9467**	4.014	0.4014	0.6206	0.5860
0.5702	1.603	0.6801	0.9172	0.9155	**0.9511**	4.156	0.3942	0.6104	0.5741
0.5848	1.631	0.6723	0.9121	0.9102	**0.9556**	4.320	0.3864	0.5990	0.5608
0.5999	1.660	0.6642	0.9067	0.9045	**0.9601**	4.515	0.3777	0.5864	0.5460
0.6155	1.693	0.6557	0.9008	0.8983	**0.9649**	4.750	0.3680	0.5721	0.5292
0.6317	1.729	0.6468	0.8944	0.8916	**0.9698**	5.046	0.3568	0.5555	0.5096
0.6486	1.768	0.6374	0.8873	0.8841	**0.9749**	5.432	0.3436	0.5358	0.4864
0.6662	1.812	0.6276	0.8766	0.8759	**0.9803**	5.976	0.3273	0.5112	0.4574
0.6845	1.861	0.6171	0.8710	0.8768	**0.9861**	6.837	0.3058	0.4783	0.4186
0.7037	1.916	0.6059	0.8614	0.8566	**0.9923**	8.609	0.2722	0.4267	0.3579

APPENDIX B

XFEM Modelling steps followed in ABAQUS

Create the cracked domain

1. Module→Part

From the main menu bar, select Part→Create. Name the part 'WheelGeometry'. Modelling space is 3D, Type is Deformable, Base feature is 'Solid' and approximate size 200. Click continue.

Draw the coordinate points that can represent the simplified geometry of the wheel and extrude to a depth of 10 mm.

To simplify/optimize the meshing process we create a series of partitions in the crack domain which separate the cracked region from the rest of the part.

Double click on the menu bar→Tools→Partition→ Face sketch→ Draw the middle section of the wheel representing the contact patch.

Partition→ cell→ Normal to edge to have three sections.

2. Module→Property

From the menu bar, select Material →Create. Name the material as **R7T steel**. And create the material property of the steel

i. General →Density
ii. Mechanical →Elasticity →Elastic: Under type choose Isotropic. Put the value of **Young's Modulus** and the **Poisson's ratio**.

    Mechanical →Plasticity →Plastic: Under type choose Isotropic. And put the value of the value in Table 4.9.
    Mechanical → Expansion (For the thermal load analysis): Under type choose Isotropic and Toggle on **Use temperature dependent data** with a reference temperature of 20^0C. Put the values in Table 4.10.
iii. Thermal → Conductivity: Under type choose Isotropic. Toggle on use temperature dependent data. Table 4.10.
iv. Thermal →Specific Heat: Under type choose Isotropic. Toggle on use temperature dependent data. Table 4.10.
v. Mechanical →Damage for Traction separation laws →Maxps Damage: Tolerance: 0.1. Put the maximum principal stress of **500 (N/mm²).** On the **Suboptions** select DamageEvolution menusection. Use Energy type damage evolution for fracture energy of 12.136 N/mm. On the **suboptions** menu again select Damage

stabilization cohesive as 0.08 for the viscosity coefficient (i.e less than fracture energy fraction comparatively).

From the Main menu bar, select →Create →Name: 'Wheel main' →category is solid, Type: Homogeneous→ Continue. In the Edit section dialogue box, under material pick R7T steel. Select the Assign section icon  and select the whole wheel entire domain then toggle **Done**. In the edit section Assignment dialog box, select wheel main, and R7T steel and click Ok.

3. Module →Mesh

Mesh →Element type→ Element library: Standard→ Type: 3D stress→Select full integration for the area of interest (or crack domain) and reduced integration for other areas and Element shape: Tet.

Mesh→ Mesh controls→ structured **tet**. For the full integration region and swept tet. For reduced integration region.

Mesh→ Seeds→ Assign seeds by number as per figure 4.15.

Part→ Assembly→ Instance→ Select wheel and accept the default then Ok.

Creating XFEM Crack

1. **Module →Part**

   Double click on Parts. Enter name as 'crack', modelling space is 3D, Type is Deformable, Base feature is Shell, Type is Extrusion and Approximate size is 200 mm. Click **Continue**.

2. Expand 'Assembly', and then double click on instances. Select 'crack' and accept the default settings by clicking ok.
3. Select 'Interaction' from the main menu, click 'Special'. Name as: 'subsurface crack' Type is XFEM and continue. Select Interaction and Name it as 'Crack Growth' type is XFEM crack growth.

Create Boundary Conditions and Loads

1. From the main menu bar, select step →Create
2. Name it step-1. The Procedure type is General →Static, general.
3. In Edit step dialog box, under the basic tab, enter **Contact Pressure** as the description. Time period is 1 second. To account for large plastic deformation, toggle on **Nlgeom**(Non-linear geometry).

And toggle on Incrementation: Type is Automatic. Maximum number of increments is **100000**. Increment size is from: **0.01** and minimum is **1E-10** and Maximum is 1.

Select **other** and General solution controller →Edit →step-1 →continue →Toggle on Specify and Time increment →I_a from **5** to more than **20**. And toggle on Discontinuous analyses. Automatic damage stabilization specify dissipation energy fraction.

To Create the Boundary Condition

For the combined thermal and mechanical analysis:

Specify the maximum temperature rise at the wheel surface by using predefined field setup i.e Select Predefined fields from the main menu bar→ Create temperature field which propagate from 20^oC to 955^oC.

1. From the main menu bar, select BC →Create: select step-1. Category is Mechanical. Type for selected step is Symmetry/Antisymmetric/Encastre. Name is Fixed End. Select the upper simplified wheel portion. Click Done and choose ENCASTRE from the Boundary dialogue box and click continue.
2. Double click on loads. Enter name as Contact Pressure, category is Mechanical, Type is Pressure, click continue. Magnitude is 506 (N/mm^2).

In order to visualize the crack in the output database the following changes need to be made to the step module:

Step module →Output →Field output requests→Manager→F-output-1→Edit → Expand Fracture/Failure →PHILSM (In order to see the crack) then State/Field/user/Time →STATUS XFEM (to see the status of the artificial crack, Propagating or static)-Put additional parameters like Von-mises stress and PEEQ (Equivalent plastic strain criterion) from Stress and strain menus.

MODULE→JOB

From the main menu bar, select Job→ Create. Enter any name for the job. Summit the job and monitor the progress. Then finally see the Results.

APPENDIX C

UIC 60 Rail Profile

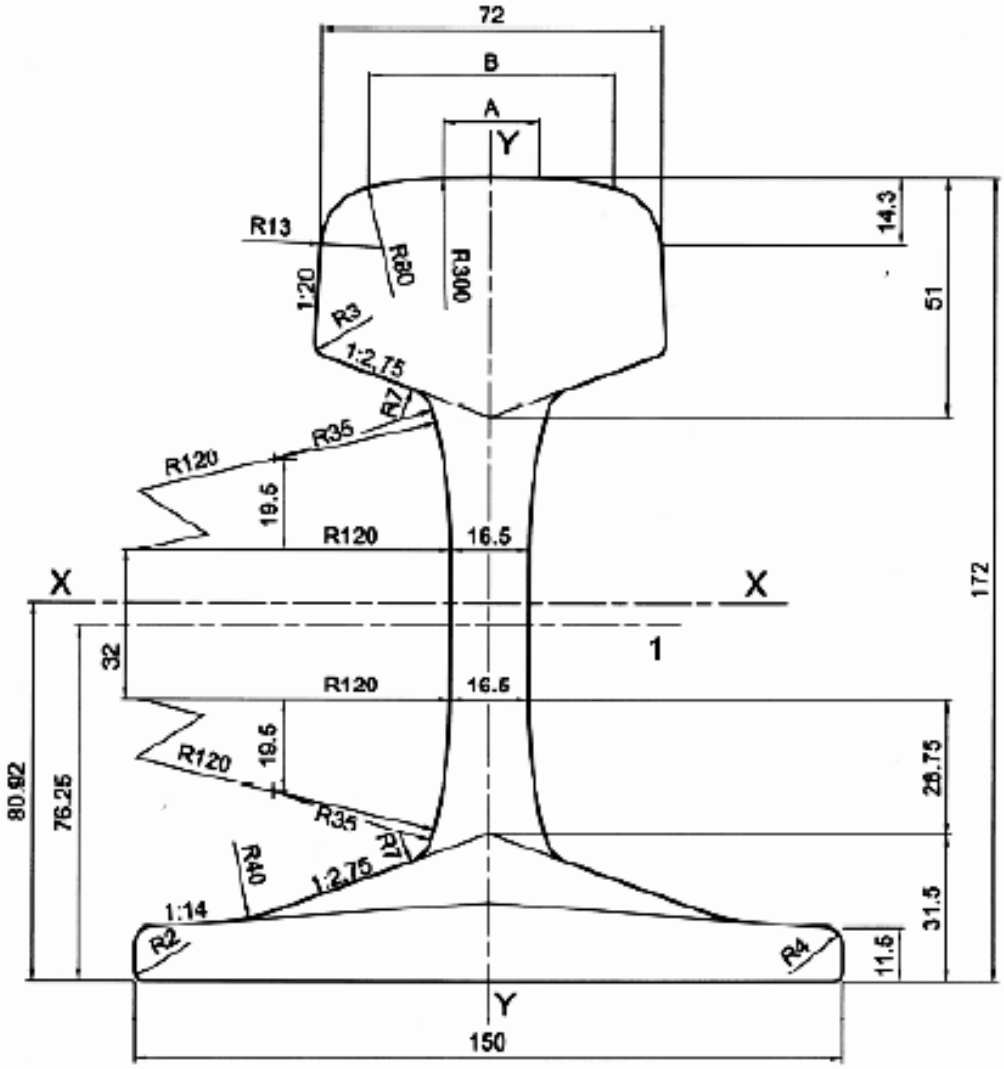

Key

1 centre line of branding

cross-sectional area	:	76,70	cm^2
mass per metre	:	60,21	kg/m
moment of inertia x-x axis	:	3 038,3	cm^4
section modulus - Head	:	333,6	cm^3
section modulus - Base	:	375,5	cm^3
moment of inertia y-y axis	:	512,3	cm^4
section modulus y-y axis	:	68,3	cm^3

APPENDIX D

UIC S1002 Wheel Profile